^{19}F Magnetic Resonance Imaging (MRI): From Design of Materials to Clinical Applications

Ilaria Tirotta,[†,‡] Valentina Dichiarante,[†,‡] Claudia Pigliacelli,[†,‡] Gabriella Cavallo,[†,‡] Giancarlo Terraneo,[†,‡] Francesca Baldelli Bombelli,*[,†,‡,§] Pierangelo Metrangolo,*[,†,‡,∥] and Giuseppe Resnati*[,†,‡]

[†]Laboratory of Nanostructured Fluorinated Materials (NFMLab), Department of Chemistry, Materials, and Chemical Engineering "Giulio Natta" and [‡]Fondazione Centro Europeo Nanomedicina, Politecnico di Milano, Milan 20131, Italy

[§]School of Pharmacy, University of East Anglia, Norwich NR4 7TJ, United Kingdom

[∥]VTT-Technical Research Centre of Finland, Espoo FI-02044, Finland

Received: May 30, 2014
Published: October 20, 2014

1. INTRODUCTION

To enable early monitoring of various diseases, to develop noninvasive diagnostic tools, and to implement targeted therapies are some of the major challenges in current medicine. Imaging techniques play a key role in the pursuit of these targets, and magnetic resonance imaging (MRI) is one of the most promising among those that do not use radioactive nuclides or ionizing radiations.

The basics of imaging by nuclear magnetic resonance (NMR) were laid by Lauterbur in the early 1970s[1] and rely upon the ability of hydrogen atoms to align and precess around an external magnetic field. Excitation by transverse radiofrequency pulses disrupts protons' magnetic alignment, influencing both their longitudinal or spin−lattice relaxation (defined as the T_1 time constant) and their transverse or spin−spin decay time (T_2 time constant). Differences in how protons relax to their ground state are then processed to reconstruct the strength of the signal arising from each imaging unit (voxel) and to generate an image. Over the years, the huge amount of mobile water in living tissues and the different relaxation properties of its hydrogen atoms has been exploited by clinical ^{1}H MRI to provide physiological and anatomical information with high spatial resolution and excellent soft tissue contrast.[2−4]

Anatomical resolution is a strength of the MRI technique, and relative insensitivity is a weakness which requires the use of tailored contrast agents (CAs). The CAs, while not directly visualized, can affect ^{1}H signals of surrounding water and thus highlight anatomical and pathological features in the imaged tissues by enhancing images contrast.[5−7] For example, Gd^{3+} or Mn^{2+} chelates, and analogous paramagnetic complexes, decrease T_1 and result in a faster signal decay and a brighter region in the image (positive or hyperintense contrast),[8] while superparamagnetic iron oxide (SPIO) nanoparticles (NPs) accelerate transverse relaxations and induce localized darker spots (negative or hypointense contrast).[9−11] Although such CAs have significantly improved MRI performance, they still present some disadvantages. First, their use generally requires longer acquisition time as it is necessary to acquire images before and after their administration; second, their localization, based on contrast modulation, is often complicated by the high background signal from water as well as by the intrinsic sources of contrast in tissues, such as blood clots and endogenous iron.[12] Furthermore, the quite low sensitivity of standard ^{1}H MRI techniques requires relatively high concentrations of such contrast agents, possibly resulting in toxicity issues.[13]

One of the most studied strategies to overcome these issues is the development of a "second color" or "hot spot" imaging using heteronuclear MRI atoms, such as ^{13}C, ^{23}Na, ^{31}P, or ^{19}F in addition to ^{1}H.[8] In this case, the magnetic resonance effect of the additional element adds a second colored layer of independent information to the anatomical details provided by the

corresponding gray-scale ^{1}H image. With its extremely favorable NMR properties, ^{19}F seems to be the most promising imaging nucleus.[14] It has 100% natural abundance and spin 1/2; its gyromagnetic ratio is very close to hydrogen (40.08 vs 42.58 MHz/T of ^{1}H), and its sensitivity is 83% of proton. Additionally, ^{19}F chemical shifts vary in a broad range (>350 ppm),[15] and only trace amounts ($<10^{-6}$ M) of ^{19}F are present in the human body. They are in bones and teeth, where they are immobilized in the solid phase, leading to a very short T_2 relaxation time and a background signal much below MRI detection limits. It thus emerges that a combined $^{19}F/^{1}H$ imaging approach—whose feasibility was first demonstrated in 1977 by Holland et al.[16]—allows for several quantitative applications, thanks to the absence of endogenous ^{19}F signals and to the linear relationship between ^{19}F content and resulting signal intensity.[17]

However, the need to administer low doses of fluorinated tracers combined with the low efficiency of T_1 may make long acquisition times necessary, and ^{19}F MRI sensitivity may become a particularly critical issue. The most straightforward strategies to enhance the contrast-to-noise ratio are to increase the magnetic field strength and to improve pulse sequences, but a tailored chemical modification of the CA is an alternative and promising approach. Use of dual-modality probes, functional targeted reporters, and large molecules bearing a high number of equivalent fluorine atoms have also been explored in the past decade.[18]

Full exploitation of ^{19}F MRI techniques for in vivo applications was limited by the initial lack of specific clinical scanners as most of them were only designed for ^{1}H applications. The possibility to modify MRI scanners, by adding a suitable ^{19}F coil and customizing the hardware (e.g., preamplifier, transmit/receive switch, and radiofrequency power amplifier suitable for ^{19}F), promoted their use in ^{19}F-based medical imaging studies.

During the years several strategies have been proposed to develop novel $^{1}H/^{19}F$ techniques,[19] the early imaging studies typically used single-frequency tunable coils, in which the coil had to be manually tuned to maximize the signal-to-noise ratio (SNR) with an undesired extension in the acquisition time. Alternatively, use of either a two-coils setup or autotuned radiofrequency coils, which can switch resonant frequency thanks to an external computer program, has been adopted for detection and quantification of fluorinated agents. These two approaches have shown some limitations in terms of sensitivity and inaccuracy in the coregistration of the $^{1}H/^{19}F$ signals.[20] In addition, an interesting improvement in the architecture of MR scanners was recently proposed by Keupp and co-workers. It relies on a method for simultaneous acquisition of dual-nuclei $^{19}F/^{1}H$ MR data in which the radiofrequency waveforms are generated in two separate transmitters and combined thanks to a specific low-power "combiner" positioned before the power amplifier. A remarkable benefit of this methodology lies in the possibility to simultaneously obtain anatomical and motion information with high SNR.[21]

The aim of this review is to give an overview of selected examples of the fluorinated tracers studied to date for imaging purposes. A special focus will be made on their chemical structures, delivery vectors, and MRI performances. We will also present the "state of the art" of their in vivo applications as diagnostic and drug delivery tools.

2. FLUORINATED TRACERS FOR ^{19}F MRI: CHEMICAL STRUCTURES AND IMAGING PERFORMANCE

As previously explained, ^{1}H MR images come from the signals of the water molecules present in biological tissues, while those of ^{19}F MR come only from the fluorine atoms contained in the used fluorinated tracers. To overcome the resulting sensitivity issue, the covalent coupling of a paramagnetic lanthanide CA to the fluorinated probe has been explored as a possible approach to improve relaxation properties.[22] Specifically, Parker and co-workers[23−25] have shown that when a trifluoromethyl group is close to a paramagnetic center (the distance being between 4.5 and 7 Å), a sensitivity improvement up to 25 times occurs. The separation between the lanthanide ion and the fluorinated unit has to be finely engineered. If the fluorinated group is located too far away from the metal ion, the relaxation rate enhancement is almost negligible, while if the fluorinated group is too close, line broadening becomes the main effect.

The molecular size of the fluorine-labeled lanthanide tracers strongly influences their fate in the body; in fact, low molecular weight CAs tend to clear from the body, resulting in a rapid reduction of the spin density in the region of interest. A strategy to slow this process relies on the synthesis of medium molecular weight and fast-relaxing fluorinated probes which are linked to a biocompatible vector. Such approach allows spectral and imaging studies to be performed at doses comparable to those of clinically approved proton CAs.[26]

Moreover, several efforts have been made in the development of new specific pulse sequences aimed at improving MRI performances.[18] Accelerated imaging has been pursued by rapid small angle excitation using gradient echoes or echo volume methods.[27] A very recent approach to reduce the MRI acquisition time is the compressed sensing where sparse signals may be effectively detected.[28]

Alternatively, a high density of ^{19}F nuclei in the tracer and a high tissue concentration of the tracer can also be employed to generate a good-quality image. Perfluorocarbons (PFCs), namely, organic compounds in which all hydrogen atoms are replaced with fluorine, are the agents most commonly used for ^{19}F MRI applications when the latter approach is pursued.[29,30]

Thanks to the strength of the C−F bond and the high electronegativity and low polarizability of fluorine, PFCs exhibit high thermal, chemical, and oxidative stability, low polarity, weak intermolecular interactions, high vapor pressure, and small surface tension. They are highly hydrophobic and significantly lipophobic; therefore, they have a tendency to segregate from the surrounding environment independently of its chemical nature.[31−39] These very peculiar physical and chemical features determine unique biological properties, which made these compounds highly attractive for some specific applications in medicine. PFCs are the most biologically inert organic xenobiotics and tend to be nontoxic in vivo, even at high doses. Typically they are not degraded at physiological pH values, are generally not metabolized by enzymes, and tend to be cleared via the reticuloendothelial system and excreted through the lungs by exhalation.[40] Moreover, fluorine being covalently bonded to the administered tracers, these molecules tend to be more stable than the lanthanide-based CAs, and the risk of false positives and toxicity, due to unbound metal ions, is reduced. When in vivo applications are pursued, PFC derivatives need to be formulated into tailored delivery vectors in order to overcome their low water solubility, to obtain injectable preparations, and to optimize their clearance profile. Specific strategies have been

developed to reach these targets, and they vary depending on the nature of the fluorinated probes and the pursued application.[41]

While some chemical properties of PFC derivatives are largely unaffected by their structure, this is not the case for their MRI performances, and the exact chemical structure of a fluorinated tracer is of paramount importance in the design of an optimized agent. The "perfect" tracer should be characterized by (i) high fluorine content, (ii) facile, and possibly scalable, synthesis and formulation, (iii) definite chemical properties, (iv) chemical and biological stability, possibly with a long shelf life, (v) low in vitro and in vivo toxicity, (vi) simple ^{19}F NMR spectrum, possibly with a single, sharp, and intense peak, and (vii) short T_1 and long T_2.

With this in mind, the currently known ^{19}F MRI agents have been grouped in the following paragraphs according to their chemical structure and divided in three broad groups: molecular tracers, polymers, and (hyper)branched derivatives. Specific sections have been devoted to fluorinated inorganic NPs and multimodal imaging probes that offer the possibility to combine MRI with other diagnostic techniques (e.g., optical imaging).

2.1. Molecular Tracers

The easiest choice for a ^{19}F probe is obviously a small fluorinated molecule that is commercially available and allows for quantitative application as its amount in MRI experiments can be exactly determined. Early works reported in the literature were thus focused on this kind of molecules[42,43] with hexafluorobenzene (HFB),[44,45] perfluorodecalin (PFD),[46,47] and perfluorononane (PFN; Figure 1) being the more frequently used derivatives.[48]

HFB was found to exhibit exceptional in vivo sensitivity to changes in oxygen tension.[44] When administered in central and peripheral regions of rat breast tumors it served as a valuable ^{19}F MRI reporter molecule; oxygen tension maps were achieved, and the correlation between tumor vascular oxygenation and tissue oxygen tension dynamics was investigated.[45] Perfluorodecalin (PFD), widely used as a blood substitute and for liquid-assisted ventilation,[46] has been tested as an alternative and nontoxic PFC for in vivo inflammation imaging, although very weak signal intensities were obtained.[47] Perfluorononane (PFN) proved to be a well-tolerated and biologically inert oral CA for in vivo gastrointestinal imaging.[48]

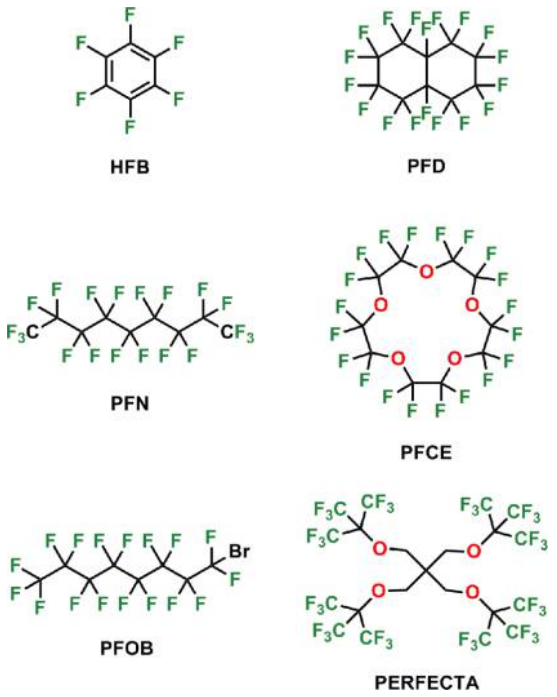

Figure 1. Chemical structures of some ^{19}F molecular tracers: hexafluorobenzene (HFB), perfluorodecalin (PFD), perfluorononane (PFN), perfluorooctyl bromide (PFOB), perfluoro-15-crown-5-ether (PFCE), and tetra(perfluorotertbutyl)pentaerythritol (PERFECTA).

Research efforts on molecular tracers then focused mainly on perfluorooctyl bromide (PFOB; a linear PFCs) and perfluoro-15-crown-5-ether (PFCE; a macrocyclic compounds) (Figure 1).

PFOB (also known as Perflubron) is a commercially available linear PFC bearing 17 fluorine atoms, which started to gain prominence in the early 1990s.[49,50] It is a hydrophobic and dense liquid, has a low diffusion coefficient into blood, and displays an enhanced clearance rate from the body, as a likely consequence of the presence of bromine.[41] PFOB poses minimal toxicological risks, since it is extremely inert and stable,[51] its clearance from circulation in mammals takes place mainly in the liver and spleen, and ultimately it is eliminated by lungs through exhalation.[52] Other useful properties which enable PFOB to function as a robust contrast agent are its magnetic susceptibility, low surface tension, high specific gravity, and water immiscibility.[50] It has been used for years in liquid ventilation[53,54] and as a contrast agent for computed tomography and ultrasonography[52] and was also the first linear PFC used for in vivo MRI of reticuloendothelial system.[55] Thanks to its high biological inertness, PFOB proved to be safe for MRI of the abdomen and pelvis in a phase III clinical trial.[56] Furthermore, this tasteless and odorless liquid is not absorbed at all from the gastrointestinal tract, so that its ingestion in liter-size doses for bowel imaging has been approved by the U.S. Food and Drug Administration (FDA).[57]

The ^{19}F spin−lattice relaxation rate of perfluorooctyl bromide is linearly dependent on the partial oxygen pressure (pO_2) at a given temperature, with its CF_3 resonance being particularly sensitive to pO_2.[58] Along with these favorable relaxivity parameters, the PFOB ^{19}F NMR spectrum shows eight peaks, one for each CF_n moiety, a detrimental feature in terms of signal-to-noise ratio and imaging quality. To minimize artifacts when using PFOB, MRI pulse sequences often incorporate presaturation radiofrequency (RF) pulses on undesired resonance peaks in order to suppress them.[59] A multispin echo (MSE) sequence optimized for PFOB imaging has been recently developed by Giraudeau and co-workers and yields an excellent sensitivity in vitro.[60] It suppresses J coupling between the different resonances of PFOB molecules thanks to selective refocusing of the CF_3 resonance; as a result, signals from CF_2Br and CF_2 groups are eliminated.

A better NMR performance can be achieved with some macrocyclic perfluoropolyethers, e.g., the 12.4, 15.5, or 18.6 crown ethers. The physical-chemical properties of these compounds are similar to those of the previously mentioned liquid PFCs, but with their high number of equivalent fluorine atoms (16, 20, and 24, respectively), they eliminate the risk of chemical shift artifacts, allow for an unambiguous identification of the PFC, maximize SNR, and, importantly, provide a single sharp resonance peak. Thanks to its 20 chemically equivalent fluorine atoms that give one single ^{19}F NMR signal at −92.5 ppm, the 15.5 isomer (PFCE) has been widely investigated as ^{19}F MRI contrast agent, in particular for cell tracking and targeted drug delivery purposes.[61] In recent years this macrocyclic compound is gaining more and more interest if compared to PFOB, despite the scarcely available toxicity data that prevent its use in humans.

PFCE was recently studied as a fluorinated reporter probe for in vivo dynamic assessment of muscle oxygenation (in mice).[62] In this work, it proved to be well suited for chronic measurements of pO_2, since it showed a quickly fading tissue toxicity, and no repeated injections of the probe were required thanks its long half-life and SNR.

Formulation of PFCs as oil-in-water (o/w) nanoemulsions is the most widely used strategy to overcome their poor water solubility. Usually such colloidal systems consist of nanodroplets with a PFC core coated by a lipid layer (Figure 2) and can be

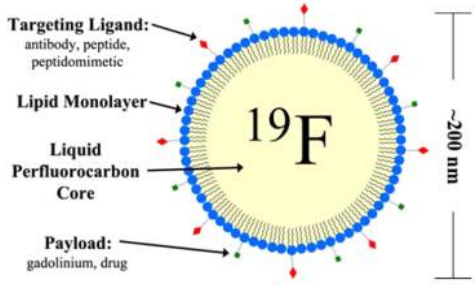

Figure 2. Cartoon representing a multifunctional PFC nanoemulsion droplet. The PFC core is coated by a lipid monolayer which can be functionalized with specific targeting and payload molecules. Reprinted with permission from ref 52. Copyright 2009 Springer Science.

stabilized by different emulsifiers (see Table 1). These agents reduce the excess interfacial energy and form a structural–mechanical barrier around PFCs particles, preventing them from sticking together.[41,63,64] However, the final PFC concentration and the stability of the resulting emulsions are highly dependent on the chemical nature of the used PFC. While high concentrations of PFCE can hardly be achieved, it is possible to prepare very stable and concentrated emulsions of PFOB. For example, egg yolk phospholipids (EYP) serve effectively this purpose as they lower the PFOB/water interfacial tension and afford an optimal hydrophilic–lipophilic balance value.

The most common emulsifiers for in vivo applications include surfactants such as pluronics (also called poloxamers) and phospholipids. The former are synthetic neutral block copolymers, made of a central polyoxypropylene hydrophobic chain and two polyoxyethylene hydrophilic side chains,[65,66] which provide a steric barrier against coalescence of PFC particles. Among them, Pluronic F68 was the most used in first-generation PFC emulsions, due to its low acute toxicity and metabolic inertness.[41] Natural phospholipids from egg yolks, soybean, etc. (e.g., lecithin), allow one to obtain better emulsion stability and fewer side effects than pluronics. Surfactant–lipid comixtures are also often used. A typical example is safflower oil with cholesterol and/or glycerin, but even more exotic comixtures have been employed, e.g., phospholipids and partially fluorinated alkanes.[67] Polyethylene glycol (PEG, 0, 5, or 50% w/w) can be incorporated in order to improve the stealth of PFOB nanoparticles and prevent nonspecific protein adsorption and cell adhesion.[68] Typically emulsions are obtained via direct sonication, microfluidization, or high-pressure homogenization and have a droplet size below 200 nm, with a high monodispersity (polydispersity index (PDI) < 0.2) and stability to dilution in various media.

As mentioned above, PFOB has already been approved for clinical use, but the latest trend in ^{19}F MRI seems to prefer PFCE due to its more favorable NMR properties. Two main formulation strategies have currently been reported for this tracer. The first and more straightforward formulation was proposed by Ahrens' group. It optimizes the ^{19}F MRI performances by maximizing the fluorine content of the emulsion thanks to addition of lecithin and safflower oil.[61] The approach investigated by Wickline and co-workers is more complex and focuses on development of more flexible multimodal probes in which the PFCE core is surrounded by a multifunctional layer containing targeting ligands, drugs, dyes, etc.[69] Typically, the surfactant–lipid comixture comprises also a lipophilic gadolinium chelate (e.g., Gd–DTPA–BOA) to influence ^{19}F relaxivity.

Conjugation of these nanoemulsions to other agents is often pursued to improve their MRI performance or to obtain a multimodal functionality (see section 4). In this perspective, an innovative approach is the replacement of lipid surfactants with biodegradable polymeric coatings, which can host liquid PFCs in their hydrophobic cores. Poly(D,L-lactide-*co*-glycolide) (PLGA), for example, is already FDA approved for human use, it is easily degraded and metabolized in vivo, and can be targeted in vivo using antibodies or other ligands.

In 2010 a biodegradable PLGA coating able to encapsulate and stabilize various PFCs was reported by Srinivas et al.[70] NPs containing PFD, perfluorohexane, perfluorooctane, PFOB, or PFCE, having an average size between 220 and 320 nm and PDI < 0.3, were prepared and subsequently coated with positively charged oligomers; an antibody was also covalently bound to their surface. The best in vivo imaging performance was achieved with PLGA–PFCE particles, which gave the highest PFC encapsulation. The PLGA polymeric shell was claimed to increase the system stability and mechanical strength in comparison to standard emulsions.

A similar approach was later used by Fattal and co-workers in the preparation, via an emulsion–evaporation process, of PLGA–PEG nanocapsules containing a PFOB liquid core.[71] The resulting particles showed an average size of 120 nm and PDI < 0.18, together with 85% encapsulation efficiency and smooth surfaces at SEM analysis. In vivo imaging of murine colon carcinoma cells with PFOB proved to be effective. In addition, polymer chemistry allowed further functionalization with targeted ligands, and a loading compartment was made available in the shell for any lipophilic drug.

It has to be observed that even if several improvements have been made PFC emulsions still suffer severe shortcomings, including droplets heterogeneity, instability, split ^{19}F signals, and complex formulation procedures. Their efficacy is often limited in time by phenomena leading to emulsions degradation, like flocculation, coalescence, creaming, or Ostwald ripening of the nanodroplets (a molecular diffusion phenomenon that results in gradual growth of larger particles at the expense of smaller ones).[41,63,64] Moreover, both PFOB and PFCE are characterized by a relatively small fluorine content, their T_1 and T_2 values are largely influenced by tissue oxygenation, and their molecular structure cannot be further functionalized without dramatically altering their MRI or biological performances. For these reasons, even though the application of these simple fluorinated tracers in tissue oxygenation measurements remains widely spread, in recent years research efforts on fluorinated imaging agents have focused on more complex and often multimodal derivatives, as detailed in the following sections.

Table 1. Selected Examples of PFC Nanoemulsions for ^{19}F MRI

^{19}F component	dispersing agents	additives	formulation technique	size (nm)[a]
PFOB	lecithin[157]	glycerin + vitronectin or collagen III antagonist + Gd-DTPA-BOA + Alexafluor 488	microfluidization	250−320
	lecithin[158]	glycerin + Alexafluor 594 + $\alpha_v\beta_3$-integrin antagonist conjugated to PEG_{2000}-phosphatidylethanolamine	microfluidization	200
	lecithin + cholesterol[126]	Gd−DTPA−BOA + Doxorubicin or Paclitaxel + biotinylated phosphatidilethanolamine	microfluidization	250
	lecithin + cholesterol[122]	Gd−DTPA−BOA + biotinylated antifibrin monoclonal antibodies	sonication + high-pressure microfluidization	280
	lecithin + cholesterol[151]	integrin antagonists + Gd−DOTA−PE	microfluidization	280
	lecithin + cholesterol[159]	Gd−DTPA−BOA + *N*-[{ω-[4-(*p*-maleimidophenyl)butanoyl]amino}PEG_{2000}]1,2-distearoyl-*sn*-glycero-3-phosphoethanolamine + $\alpha_v\beta_3$-integrin peptidomimetic antagonist + DPPE	microfluidization	250
	chicken egg lecithin + cholesterol[119]	glycerin + $mPEG_{2000}$-PE + CdSe/ZnS QDs	sonication + homogenization + microfluidization	280
	lecithin + safflower oil + cholesterol[175]	glycerin + lissamine rhodamine B sulfonyl or nitrobenzoxadiazole (NBD)	microfluidization	220
	lecithin + safflower oil + cholesterol[123]	glycerin + Gd−DTPA−BOA	microfluidization	270
	egg yolk phospholipids[47]	$C_6F_{13}C_{10}H_{21}$ (stabilizer)	microfluidization	150−360
	phospholipids[153]	rhodamine DSPE-PEG-RGD peptide		190[b]
	PLGA−PEG copolymer nanocapsules[71]		emulsion−evaporation	120
PFCE	lecithin + safflower oil[61]		microfluidization	100−200
	purified egg lecithin[162]	glycerin + phosphate buffer		320
	purified egg lecithin[155,156]	Lissamine rhodamine B	high pressure homogenization	130
	lecithin + cholesterol[122]	Gd−DTPA−BOA + biotinylated antifibrin monoclonal antibodies	sonication + high pressure microfluidization	240
	chicken egg lecithin + cholesterol[119]	glycerin + $mPEG_{2000}$-PE + CdSe/ZnS QDs	sonication + homogenization + microfluidization	260
	lecithin + (biotinylated) dipalmitoylphosphatidylethanolamine[69]	glycerin + Gd−DTPA−BOA	microfluidization	170−230
	egg yolk phospholipids[47]		high-pressure homogenization	70−130
	egg phosphatidylcholine + dipalmitoylphosphatidylethanolamine[152]	glycerin + peptidomimetic vitronectin antagonist + Lissamine Rhodamine B	microfluidization	n.a.
	distearoyl-*sn*-glycero-3-phosphocholine + PAP (4-pyridylacetic palmitate)[112]	tetraethyl orthosilicate + rhodamine B isothiocyanate	homogenization + sonication	75
	DSPC (1,2-distearoyl-*sn*-glycero-3-phosphocholine) + cholesterol[115]	Gd−DOTA−DSPE + PEG_{2000}-DSPE + Mal-PEG_{2000}-DSPE + cyclic RGD peptide	high-pressure microfluidization	170
	phosphatidylcholine + cholesterol +1,2-dioleolylphosphatidylphosphoethanolamine (DOPE) + 1,2-dioleoyl-3-trimethylammonium propane (DOTAP) or dipalmitoylphosphatidylserine[144]	glycerin + rhodamine phosphatidylethanolamine	microfluidization	160−210
	PLGA[70]	carboxyfluorescein	sonication	240[c]
PFPE (linear PFPE glycol)	Pluronic[73]	dialkylcarbocyanine dye (DiI)	probe sonication	100
	Pluronic L35[74]	Alexa647	probe sonication	120
	Pluronic P105 + Cremophor (CrEL)[131]	NIRF dye (CellVue NIR815 or Burgundy) + Celecoxib + Miglyol 810N (GRAS medium-chain triglyceride)	microfluidization	160
FBPA (fluorescent blended PFPE amide)	Pluronic F68[76]	linear polyethylenimine (PEI) + PFPE oxide + FITC/Alexa647/BODIPy-TR	high-pressure microfluidization	160−190

Table 1. continued

^{19}F component	dispersing agents	additives	formulation technique	size (nm)[a]
CBPA (cyanine blended PFPE amide)	Pluronic F68[146]	PEI + cyanine dyes (Cy3, Cy5, CypHer5)	microfluidization	150−175
PFPE-tyramide	Pluronic F68 and P105 + CrEL[132]	Miglyol 812 + Celecoxib + CellVue NIR815 dye	microfluidization or sonication	180

[a]Sizes are expressed as hydrodynamic diameters obtained from dynamic light scattering measurements. [b]peptide excluded [c]highest encapsulation

2.2. Polymeric Tracers

Linear fluorinated polymers are the simplest choice to achieve an increased fluorine content in CAs. They can be single polymers or mixtures characterized by different levels of polydispersity. Most of the papers on polymeric ^{19}F MRI probes are using linear perfluoropolyethers (PFPEs), viz. long-chain polyethers in which all of the hydrogens have been replaced with fluorine atoms. All of these compounds have similar physical-chemical properties, being highly hydrophobic and mildly lipophobic oils, characterized by high boiling points and low surface tension, high molecular weight (>1700 Da), and high fluorine concentration (on average 40 ^{19}F atoms per molecule). Their spectroscopic properties are also quite similar, presenting one main peak around −92 ppm ($-CF_2O$) and smaller peaks due to the terminal fluorinated groups, quite short T_1, and sufficiently long T_2.[72]

The first reported works used simple linear PFPE polymers (Figure 3),[73,74] which were formulated using different pluronic

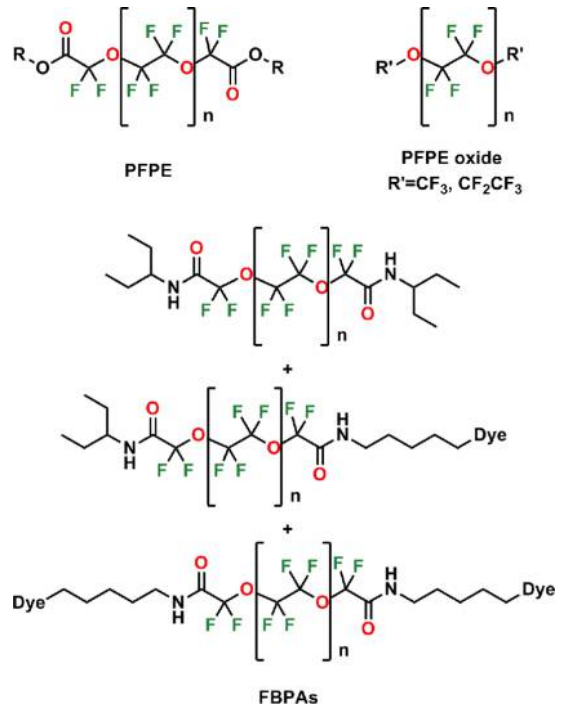

Figure 3. Chemical structures of perfluoropolyether (PFPE), PFPE oxide, and fluorescent blended PFPE amides (FBPAs).

surfactants and shear force (sonifier cell disruptor) to gain o/w nanoemulsions with droplets having a mean particle size between 100 and 120 nm and PDI < 0.2. Different ratios between the PFPE and the surfactant were used. Lipophilic fluorescent dyes were also added and found in the outer shell of the droplet. These formulations, commercially available under the name of V-Sense (Cell Sense Inc.), can be administered intravenously and have already been used in several in vivo studies.[75]

Ahrens and co-workers reported in 2008 one of the most interesting formulations, and it was based on chemically modified PFPEs.[76] Their methyl esters were converted into the corresponding ethylene amides and then reacted with different fluorescent amines to give a mixture of fluorescent blended PFPE amides (FBPAs; Figure 3). Chemical modification of the PFPE allowed the fluorescent tag to be covalently bound to the fluorinated molecule in order to achieve better control of the two

probing functions and to follow the fluorescent tag emission inside the cells. This polymeric blend was then emulsified in water using PFPE oxide (perfluoropoly(ethylene glycol) dialkyl ether), pluronic F68, a linear polyethylene imine (PEI), and a high-pressure microfluidizer. A stable nanoemulsion of 160−190 nm average particle size and PDI < 0.15 was obtained.

Different versions of this formulation are now commercially available under the name of Cell Sense. They have become the current standard for ^{19}F MRI cell tracking and have been approved by the FDA and used in several clinical trials on human patients.[77] Generally, PFPEs imaging strength is related to the high fluorine content and stability of their nanoemulsions. Minuses are related to the polydispersity of polymeric mixtures and the resulting presence of several peaks in their ^{19}F spectra; pluses are related to the very low toxicity and a proven biocompatibility with several cell lines.

As already seen in the previous section for simpler probes, an equally interesting approach to fluorinated tracers makes use of chemically cross-linked nanoparticles of fluorinated polymers. In 2012 Berkland and co-workers[78] reported the synthesis of polymeric NPs via copolymerization of two different fluorinated monomers with *N*-vinyl formamide, which was then hydrolyzed to give free reactive sites for further functionalization (Figure 4). The obtained NPs had an average size of 280 nm, sharp single peaks at ^{19}F NMR were claimed, but no MRI study was conducted.

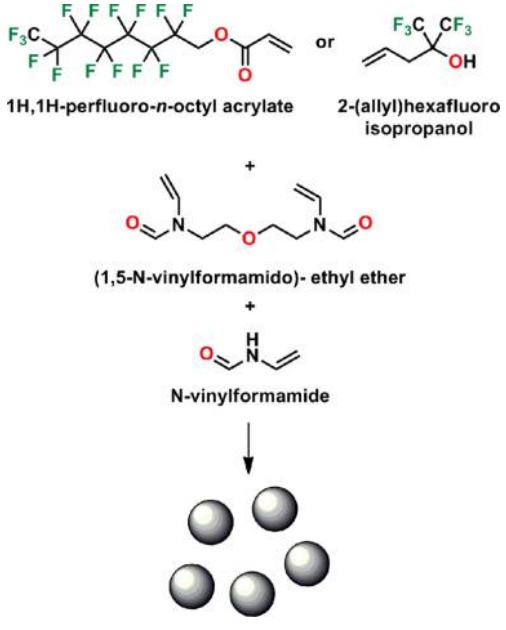

Figure 4. Synthetic route to polymeric cross-linked NPs via copolymerization of fluorinated monomers.

Another work that explored the potential of self-assembling linear fluorinated polymers as ^{19}F MRI agents[79] employed polyelectrolytes that were statistical or block copolymers of 2,2,2-trifluoroethyl methacrylate (TFEMA) and 2-(dimethylamino)-ethyl methacrylate (DMAEMA) either directly dissolved in water or assembled into aqueous NPs with kinetically frozen PTFEMA cores and P(TFEMA-*co*-DMAEMA) coronas (Figure 5). Both the size and the MRI performance of the resulting NPs showed a strong dependency on pH. Phantom analyses revealed T_1/T_2 values suitable for both in vitro and in vivo ^{19}F MRI applications, which have not been explored, yet.

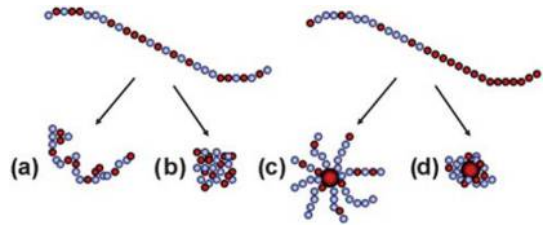

Figure 5. Representation of possible arrangements assumed by fluorinated hydrophobic (left) and block (right) polyelectrolytes in aqueous solution: (a) Extended coil, (b) compact globule, (c) extended nanoparticle, and (d) compact nanoparticle. Reprinted with permission from ref 79. Copyright 2010 Royal Society of Chemistry.

It appears quite clearly that this field is still largely unexplored, and further work is needed to make these encouraging preliminary results into actual biological applications.

2.3. (Hyper)branched Compounds

Branched probes with several perfluorinated groups on their surface and a very high fluorine nuclei density can in principle afford enhanced sensitivity and better imaging performance than linear perfluoropolymers. ^{19}FIT (^{19}F imaging tracer; Figure 6), a

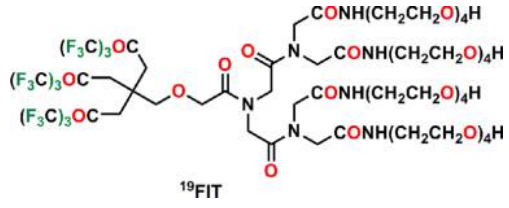

Figure 6. Chemical structure of ^{19}FIT. The molecule contains a F-hemispherical region and an H-hemispherical region.

bispherical fluorocarbon molecule developed by Yu and co-workers, is a remarkably simple example of this category of compounds.[80] ^{19}FIT is a water-dispersible waxy compound which forms micelles in phosphate buffer solutions (PBS). It bears 27 equivalent fluorine atoms, giving a single ^{19}F signal at −71.05 ppm with a considerably short T_1. Synthesis of ^{19}FIT proceeded from the F sphere to the H sphere through sequential deprotection/condensation cycles (Figure 6).

Phantom MRI experiments at 3 T showed a detection limit of 126 mM ^{19}F atom concentration, and in vivo imaging was successfully performed on mice, with a residence half-life of about 0.5 day and no evidence of organ retention or in vivo degradation.

Fluorinated hyperbranched polymers with higher fluorine content have been also developed. In 2008 Wooley and co-workers reported a series of amphiphilic hyperbranched fluoropolymers ($M_n \approx 100$ kDa; Figure 7) obtained by grafting TFEMA and *tert*-butyl acrylate, in different ratios, to a star-like core of 4-chloromethylstyrene, lauryl acrylate, and 1,1,1-tris(4′-(2″-bromoisobutyryloxy)phenyl)ethane, previously synthesized via atom transfer radical self-condensing vinyl (co)-polymerization (ATR-SCVCP).[81] Such polymers were self-assembled into micelles in aqueous solution (hydrodynamic diameters 20−25 nm). For all of them ^{19}F MRI phantom imaging showed a narrow single ^{19}F resonance signal, sufficiently short T_1, but also quite short T_2, which resulted in an acceptable SNR, linear with fluorine concentration. However, the fluorine contained in these micelles is still quite far from the amount

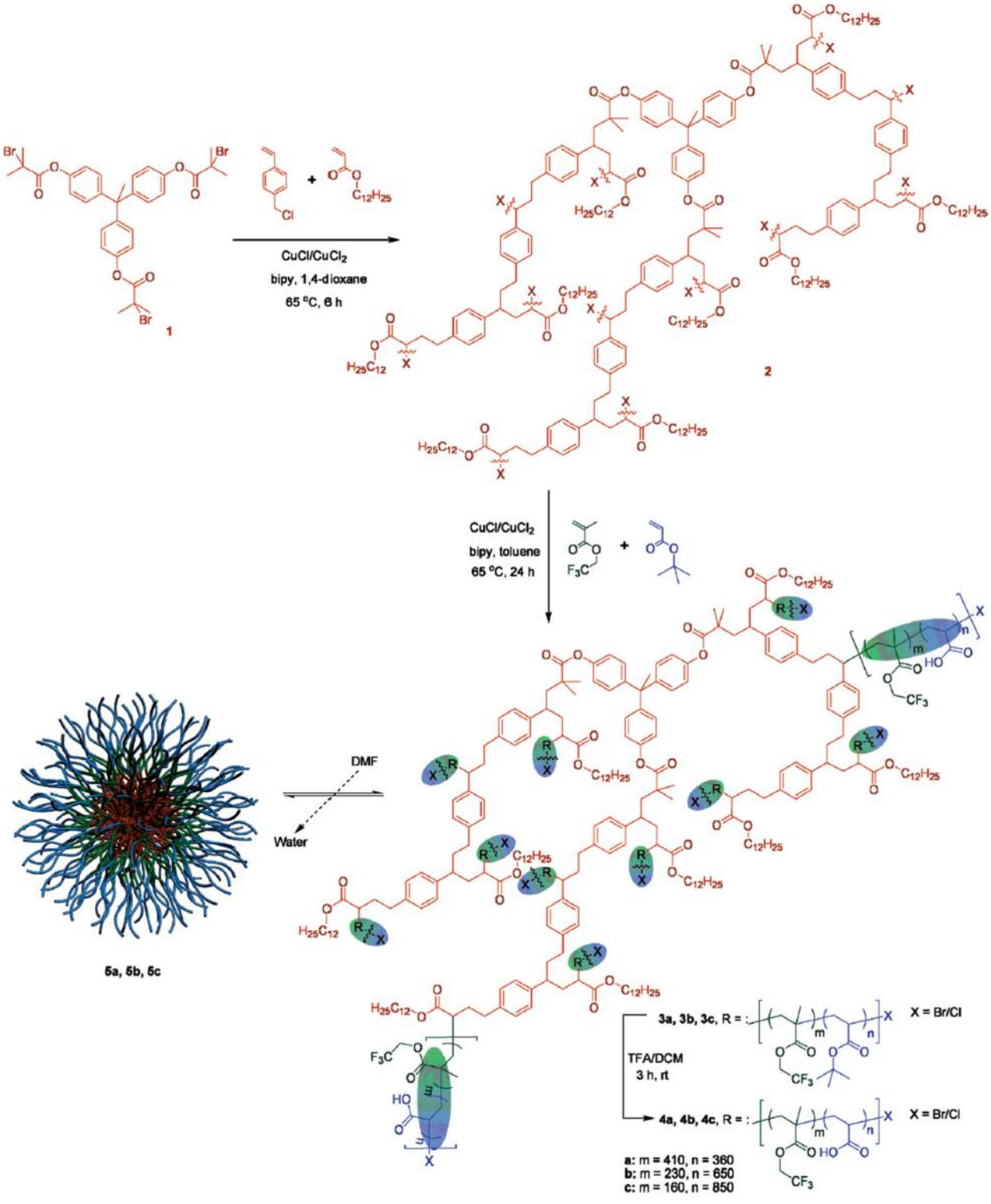

Figure 7. Schematic representation of amphiphilic hyperbranched fluoropolymers self-assembly into micelles in aqueous solutions. In **5a**, **5b**, and **5c**, the red core units represent the hydrophobic lauryl acrylate and *p*-chloromethylstyrene-based components, while the green and blue chains represent the trifluoroethyl methacrylate and acrylic acid copolymer branches extending from the core. Reprinted with permission from ref 81. Copyright 2008 American Chemical Society.

contained in PFC nanoemulsions, resulting in acquisition times so long that their in vivo application is impossible.

More recently, several fluorinated (trifluoroethyl acrylate) hyperbranched polymers with acid, alkyne, and mannose end groups were synthesized by Whittaker and co-workers via a slightly modified reversible addition−fragmentation chain transfer methodology (RAFT; Figure 8).[82]

Water-soluble, cytocompatible polymeric particles with 10 nm average size and good T_1 could be obtained via chain extension with polyethylene glycol monomethyl ether methacrylate

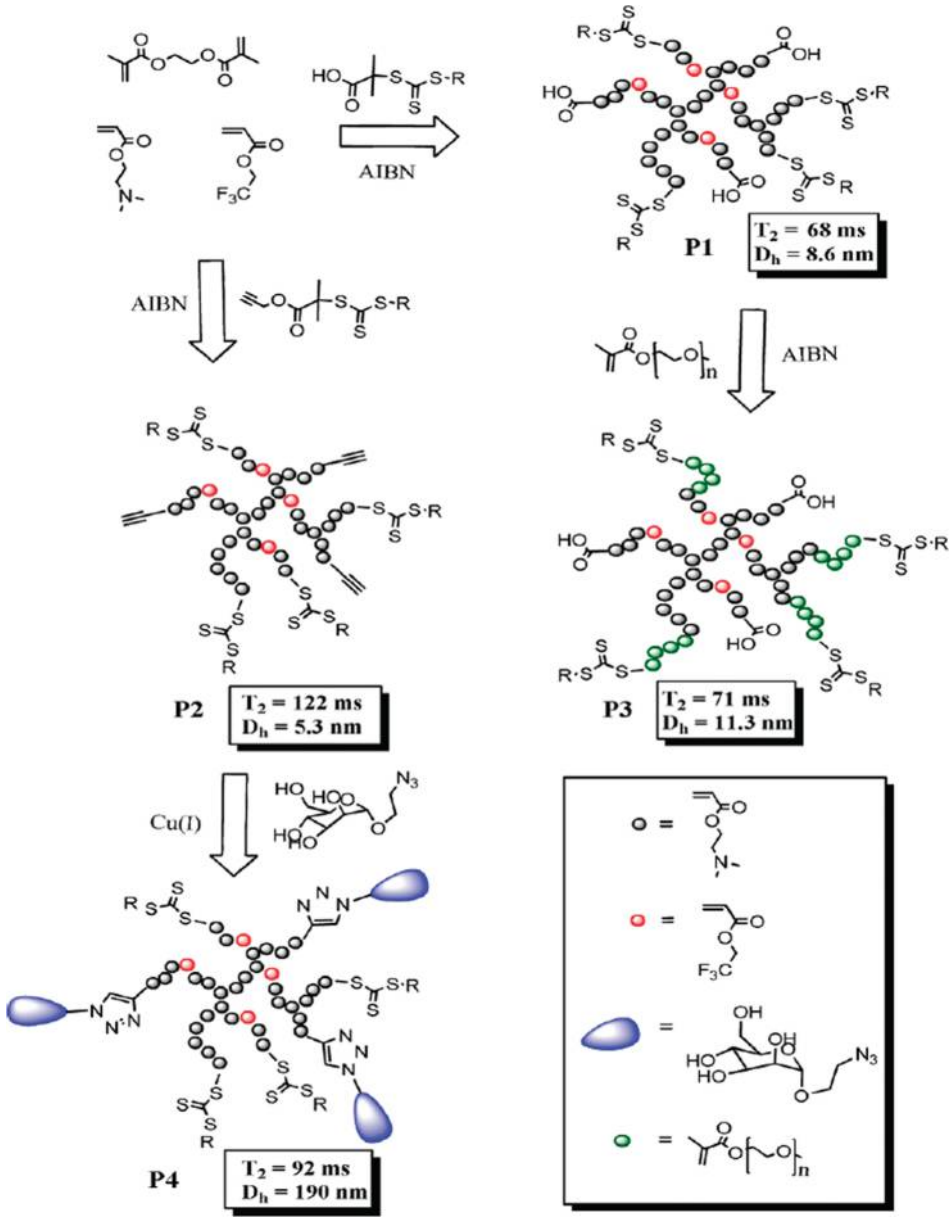

Figure 8. Synthesis of fluorinated hyperbranched polymers having acid (P1, P3), alkyne (P2), and mannose (P4) end groups. Reprinted with permission from ref 82. Copyright 2010 American Chemical Society.

(PPEGMA). Despite their quite short T_2, they could be successfully imaged in vivo in less than 10 min thanks to their high concentration. Particles conjugation to mannose derivatives via "click chemistry" was successfully pursued to prove possible further functionalization and biological application.

In a later work from the same authors a well-defined PPEGMA macro-chain transfer agent (CTA) was synthesized again through RAFT polymerization. Chain extension of this macro-CTA gave fluorinated, pH-responsive star polymers affording NPs characterized by a highly branched core and hydrophilic PPEGMA shell (Figure 9).[83]

The NPs showed a spherical morphology with a size of about 20 nm, a strong single ^{19}F peak at −72.7 ppm, and a long T_2 only at pH values lower than 6.5. Imaging of PBS solutions of such star polymers at pH 6 proved to be effective, suggesting their potential as ^{19}F MRI contrast agents. On the other hand, only irregular particles were observed above the pK_a, the T_2 value significantly decreased, and no detectable phantom images were obtained.

Showing the feasibility of the approach, this work was soon followed by a similar paper from the same group, which exploited RAFT polymerization to synthesize core cross-linked star (CCS) polymers containing TFEMA units (Figure 10) to provide ^{19}F NMR and MRI signal and 2-(dimethylamino)ethyl methacrylate (DMAEMA) segments to achieve pH responsiveness.[84]

Bis(2-methacryloyl)oxyethyl disulfide (DSDMA) is easily degraded by reducing agents, due to the presence of disulfide bonds, and NPs become highly degradable. Moreover, protonation and deprotonation of DMAEMA units influenced both the size of the NPs and the mobility of the fluorine nuclei, affecting the MRI performance of the probe. As for the previously reported derivatives, these CCS polymers were imaged well in vitro at acidic pH, while they had poor imaging performance above physiological pH. Their use as promising contrast agents

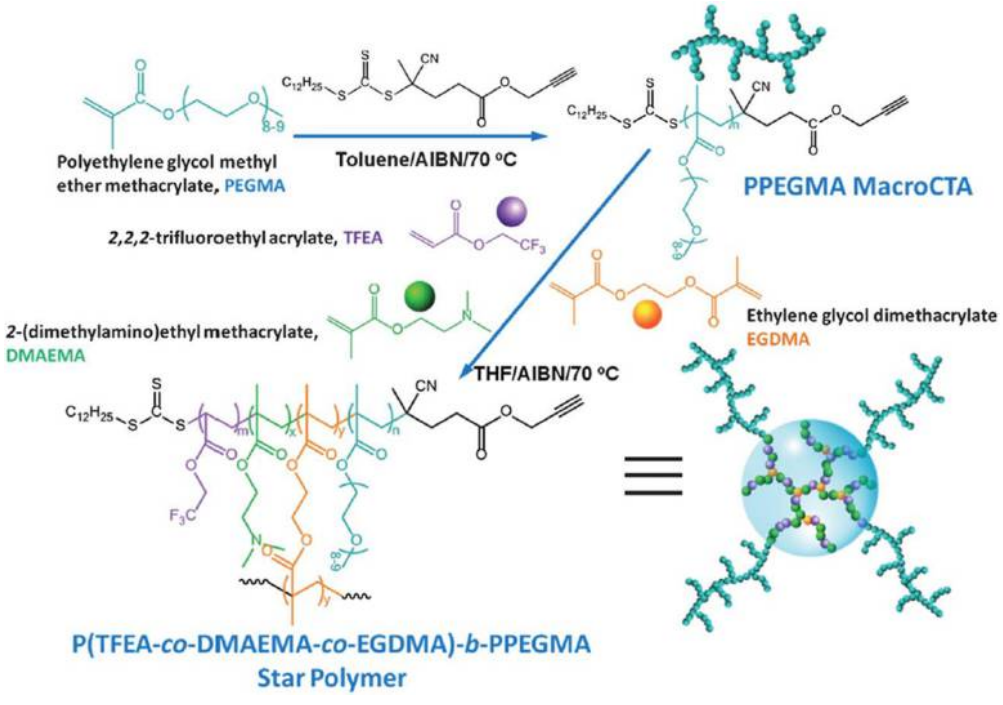

Figure 9. Scheme of star polymer synthesis. Polymeric NPs were formed in water and consisted of a highly branched core and hydrophilic shell. Reprinted with permission from ref 83 Copyright 2013 Royal Society of Chemistry.

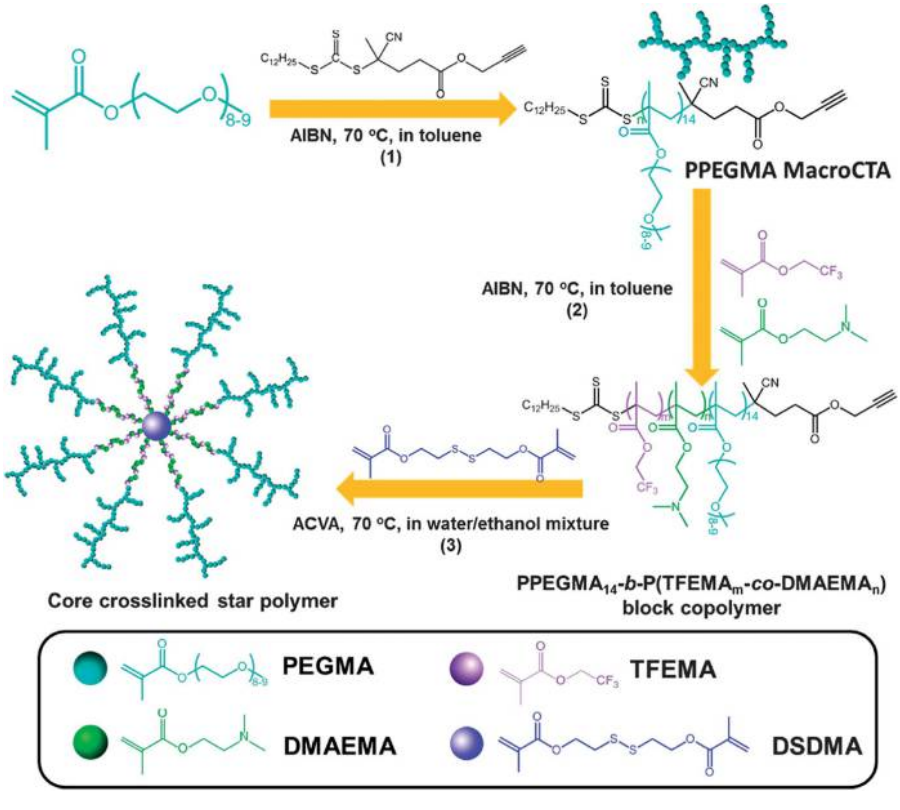

Figure 10. Synthetic scheme of CCS polymers containing TFEMA units. Reprinted with permission from ref 84. Copyright 2014 Royal Society of Chemistry.

for selective imaging of tumor tissues was suggested, although not experimentally tested, yet.

Finally, in 2014 the same group reported the design,[85] synthesis, and implementation of a new polymer-based multimodal imaging platform. RAFT polymerization was used to tailor molecular size and to allow postconjugation of different targeting ligands. Polymeric NPs, containing trifluoroethyl acrylate (TFEA), PEGMA, and ethylene glycol dimethacrylate (EGDMA) sections (Figure 11), with a size between 7 and 11

nm, were successfully conjugated with rhodamine and folate and imaged in vivo.

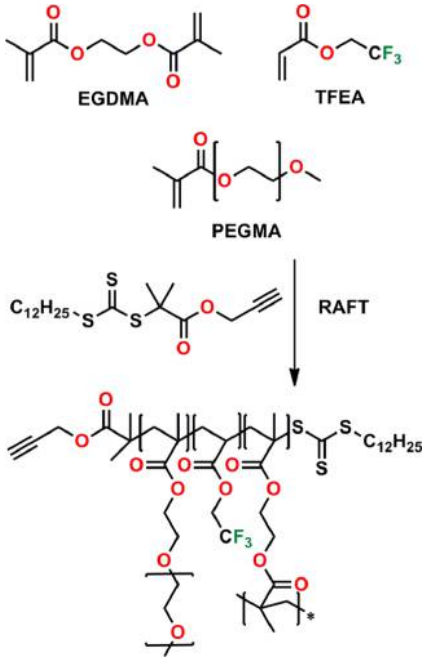

Figure 11. Synthesis, via RAFT polymerization, of polymeric multimodal NPs containing EDGMA, PEGMA, and TFEA units.

Dendrimer-like multivalent globular macromolecules (2−10 nm) with a regular and highly branched structure are an interesting class of hyperbranched polymers. Distinctive features are the many arms emanating from a central core with a well-defined number of peripheral groups. Such 3D organization and its controlled size, shape, and functional groups disposition can be obtained through a "cascade" synthesis based on an iterative sequence of reaction steps.[86−88]

From a diagnostic and therapeutic standpoint, dendrimers offer several advantages, namely, (I) low PDI, (II) prolonged vascular retention time, due to their large size, (III) multiple attachment sites for fluorinated MRI signaling moieties and targeting ligands, (IV) possibility of improving their relaxivity by modifying their periphery with gadolinium(III) chelates, and (V) a core microenvironment which is well suited for encapsulation of guest molecules.[89−91] Although the first dendrimer-based ^{1}H MRI contrast agents date back to the early 1990s,[92] only a few examples of fluorinated dendritic tracers have been reported until now.

Self-assembly of pH-responsive fluorinated poly(amidoamino) (PAMAM) starburst dendrimer-based particulates, mediated by the "fluorophobic effect", has been exploited to enable ^{19}F MRI detection of their site-specific accumulation in vivo (in mice). PAMAM(G3) dendrimers were partially fluorinated with heptafluoroacyl groups (Figure 12).[93]

The resulting products were extracted into water, and the fluorophobic effect drove spontaneous aggregation to give 1−2 μm sized adducts that were successfully imaged in vivo. T_1 of these systems significantly increases when pH decreases, and this susceptibility to pH changes is interesting for both targeted drug delivery and imaging of low-pH physiological compartments.

Another work by Ito and co-workers reported the preparation of fluorinated dendrimer polymer nanoparticles by living radical polymerization of a PAMAM(G2) macroinitiator functionalized with bromine substituents and then with 2,2,3,3-tetrafluoropropyl methacrylate (TFPMA) and TFEMA monomers (Figure 13).[94]

Resulting NPs showed an average hydrodynamic diameter in the range of 3−25 nm and sharp, often single, ^{19}F NMR peaks. T_1 values were well below the average values of low molecular weight fluorinated compounds, and T_2 values were also shorter than those of common PFCs. These results represented a proof of concept study, and no MRI application has been reported, yet.

In a later work from the same authors, a similar synthetic protocol, followed by subsequent block polymerization with carboxybetaine monomer, afforded water-soluble PAMAM-*g*-PTFPMA-*b*-PCMB NPs with a high fluorine content and biocompatibility (Figure 14).[95] Such dendrimer derivatives, having diameters in the range of 15−80 nm, showed two resonance peaks at −124 and −138 ppm and very short T_1 but still too short T_2 values.

Even though dendrimer-based agents can ensure a high number of fluorine atoms per molecule and are often characterized by a high level of symmetry resulting in intense and sharp single-resonance peaks, they require very long and elaborate syntheses and do not always allow high final fluorine

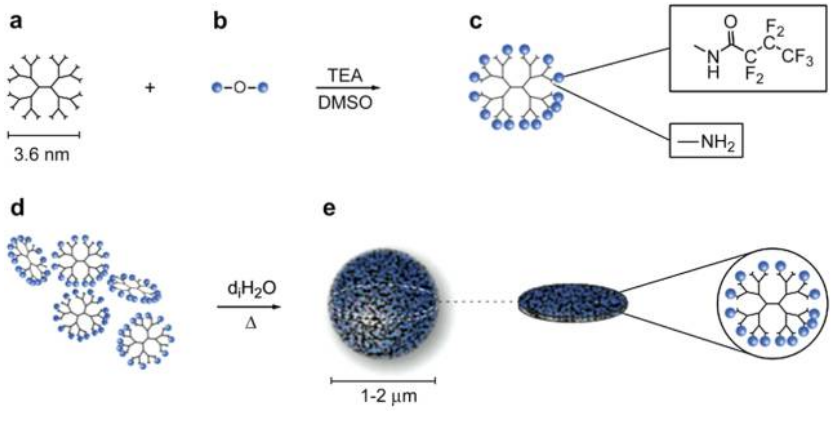

Figure 12. Schematic representation of functionalization of PAMAM(G3) starburst dendrimers (a) with heptafluorobutyric acid anhydride (b) to yield heptafluoroacylated PAMAM(G3) terminal branches (c). Partially fluorinated dendrimers (d) aggregate in aqueous solution and form self-assembled structures (e). The internal network of the obtained system is densely packed, as shown in e by the cross-sectional diameter of the particulate. Reprinted with permission from ref 93. Copyright 2009 Elsevier Limited.

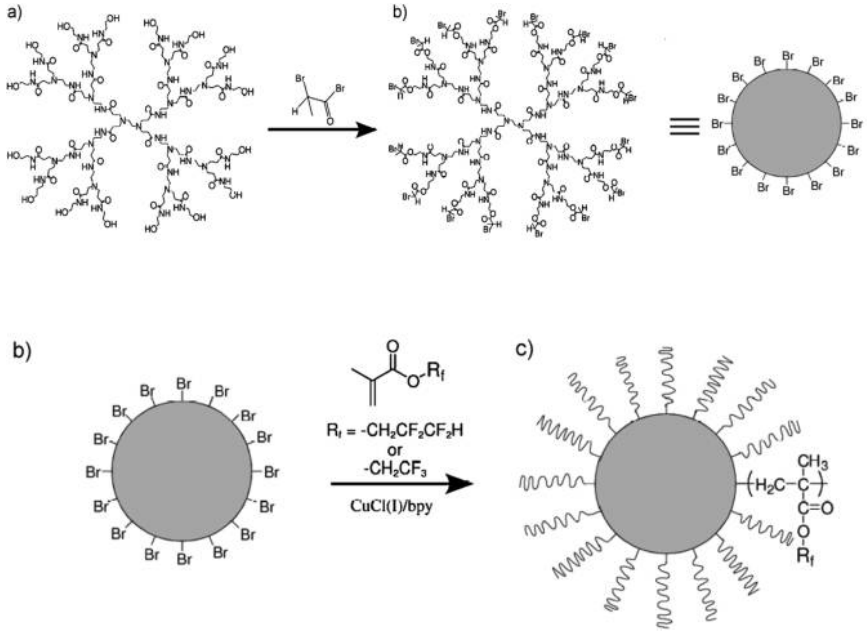

Figure 13. Synthetic scheme of fluorinated dendrimer polymer nanoparticles preparation through radical polymerization: (a) PAMAM−OH, (b) PAMAM−Br, and (c) fluorinated polymer nanoparticles. Adjusted with permission from ref 94. Copyright 2010 John Wiley and Sons.

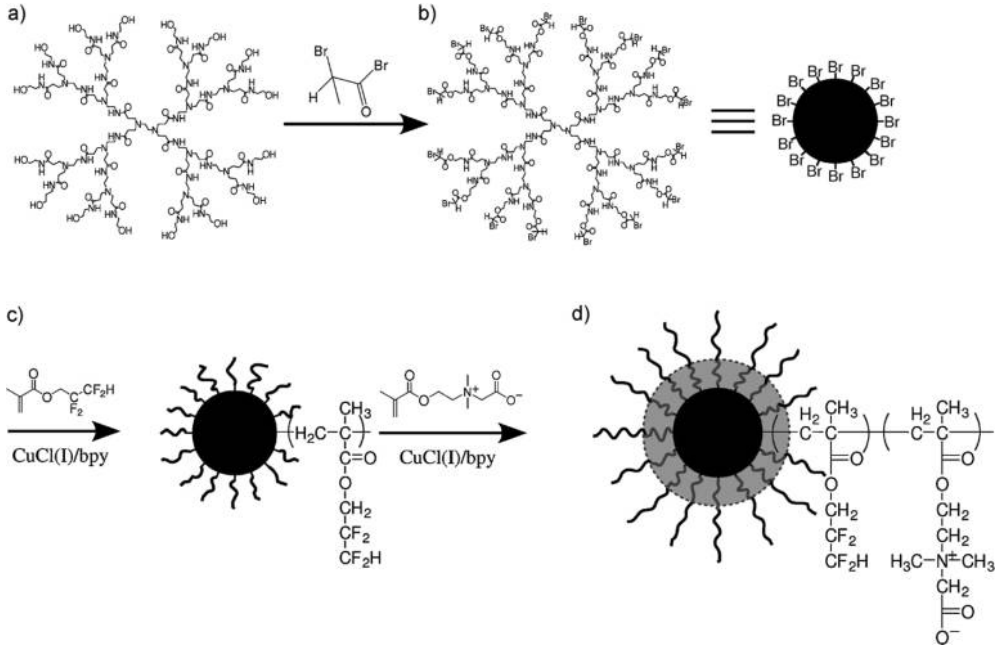

Figure 14. Synthetic scheme of water-soluble fluorinated dendrimer derivatives: (a) PAMAM−OH, (b) PAMAM−Br, (c) PAMAM-*g*-PTFPMA, and (d) PAMAM-*g*-PTFPMA-*b*-PCMB. Reprinted with permission from ref 95. Copyright 2010 John Wiley and Sons.

density. Moreover, their cytocompatibility and cellular uptake is often complex and not completely known, yet. In general, the overall toxicity of dendritic structures seems to be strongly determined by their peripheral functionalities, with cationic derivatives being the most cytotoxic ones. Cationic macromolecules, in general, and not only dendrimer ones cause destabilization of cell membranes and result in cell lysis; such hemolytic effect might be related to favorable interactions between their positive charges and the negatively charged cell membranes. The cytocompatibility of dendrimer-like structures is also reported to decrease with increasing generation number, although PAMAM dendrimers up to G5 do not appear to be toxic in vivo (in mice), independently of their surface functionalization.[96] Therefore, it is not surprising that, to date, fluorinated dendrimer MRI probes have not found concrete applications.

3. FLUORINATED METALLIC NANOPARTICLES

Use of nanotechnology for biomedical applications with both diagnostic and therapeutic purposes is one of the most rapidly growing areas of research in the 21st century.[97,98] For example, in the past decade magnetic nanoparticles (MNP) have attracted attention as contrast agents for MRI thanks to their ability to shorten T_2* relaxation times of water hydrogens in tissues.[99,100]

Much effort has been made to improve the chemical features of these NPs (e.g., size, shape, chemical functionalization) in order to target specific organs and to attain magnetic properties that better meet the clinical needs for detection and diagnosis of many diseases.[9,101,102] Additionally, MNPs have gained increased interest due to their potential use as combined hyperthermia and drug delivery systems, through development of engineered multifunctional nanoformulations (see next section).[10]

As discussed in the Introduction, the emergent use of ^{19}F MRI in biological studies resulted in an increased number of publications in the field during the past decade. A similar trend was observed in the nanotechnology field, and it is worth noting that most papers in this area describe the use of nanoemulsions and micellar suspensions of fluorocarbon molecules (see paragraph 2) rather than the synthesis of fluorinated inorganic NPs. The main drawbacks in the use of such nanoformulations as ^{19}F MRI contrast agents are related to their relatively large size (150−200 nm) and polydispersity as well as the long longitudinal T_1 times. In light of recent advancements in nanoengineering, different research groups have started to work on the development of fluorinated inorganic NPs obtaining smaller and more monodisperse fluorinated nano-objects employable for different biological applications in addition to the diagnostic use.

The work of Pasquato et al. on the synthesis of water-soluble gold NPs coated by hybrid pegylated and fluorinated ligands was the first paper on fluorinated inorganic NPs soluble in aqueous dispersions.[103] Since then, various studies pursuing preparation of fluorinated NPs agents focused on Au NPs, as their relatively easy chemical synthesis and surface functionalization allowed high yields of monodisperse NPs with sizes ranging from a few nanometers to tens of nanometers.[104−107] Functionalization of Au cores with fluorinated ligands cannot be done, in general, via the classical Brust's two-phase method,[108] which involves the use of thiols to bind the alkyl chains to the NP surface, as sulfur atoms close to a perfluorinated chain have a reduced nucleophilicity. Alternative chemical routes have thus been developed, such as the use of thiolates rather than thiols and/or phase-exchange reaction of the ligands at the nanointerface. Moreover, given the poor hydrophilicity of perfluorinated chains and their attitude to give strong fluorous−fluorous interactions, chemical strategies for further functionalization with hydrophilic groups and/or amphiphilic coating agents are necessary to finely disperse them into aqueous solutions. Most of the current work in this field has thus been focused on the optimization of synthetic protocols and characterization of these novel materials in terms of structural, physical, and chemical properties.

In 2013 Pasquato and collaborators reported MR data on water-soluble fluorinated Au NPs showing that such small nano-objects present suitable magnetic properties for their possible use as ^{19}F-MRI contrast imaging tools in vivo.[109] These promising results suggest that further work on this topic may afford new imaging nanoplatforms that can offer simultaneously multi-imaging (fluorescence, MRI, ^{19}F-MRI, PET, etc.) and therapeutic functions (see the next section). This will require producing advanced hybrid nanoparticles composed of different materials such as metal−oxides, polymers, etc., in order to join diverse properties in a unique multifunctional object. Thus far, hydrophobic magnetite and silica NPs[110−112] are the only reported examples of highly fluorinated NPs made of a material different from Au. They cannot be dispersed in aqueous solutions; thus, further efforts are needed in this direction to develop novel smart ^{19}F MRI nanoprobes.

4. MULTIMODAL IMAGING AGENTS

Much effort has been recently devoted to development of multimodal agents functionalized with different moieties bearing fluorinated probes, proton-based contrast agents, and/or fluorescent labels. This allowed different techniques (e.g., optical or tomographic imaging modalities) to be merged in one multimodal diagnostic tool. These multifunctional imaging agents combine the rapid screening offered by optical modalities with the wealth of information (physiological and anatomical) and the spatial resolution characteristic of MRI.[113] In this section we will focus on cases where the use of ^{19}F MRI is combined with other techniques and/or the use of drug molecules, and we will give an overview of the currently known approaches.

The first and simplest approach is to combine ^{19}F MRI with fluorescence detection, thus obtaining bifunctional imaging probes that can be clearly localized in vitro and/or in vivo using a simple and noninvasive technique (confocal microscopy).[114]

Highly fluorinated molecules frequently show long T_1 relaxation times and thus require long scan times. To overcome this drawback, some of the first multichromic agents were designed as a combination of fluorinated probes with paramagnetic metal ions, which have the ability to shorten T_1 values of nearby nuclei, both the protons of the surrounding water in the tissue and the fluorines of the used tracers. Paramagnetic metal ions also tend to shorten T_2, and this could result in severe line broadening.[14] Hence, the critical challenge in the design of efficient multimodal MRI agents possessing the desired performances is to find the best compromise among the different properties of all selected probes.

PFCs, such as PFOB and PFCE, have often been coupled with paramagnetic metals in order to reduce their long T_1. In 2008, Wickline and co-workers[69] reported a nanoemulsion with PFCE core, formulated with lecithin, dipalmitoyl-phosphatidylethanolamine, and bis-oleate (BOA), diethylene-triamine-pentaacetic acid (DTPA) derivatives chelating gadolinium ions. This formulation binds Gd ions to the droplet surface, and direct contact between the metal ion and the PFC core is avoided. Addition of Gd adduct into the lipid membrane of the NPs resulted in a four-times decrease of the T_1 as well as a decrease of T_2 of PFCE along with a 125% signal increase (at 1.5 T). Moreover, it was also shown that a spatial separation of the Gd unit from the NP surface influenced remarkably T_1 while minimally affecting T_2.

Similarly, Strijkers and co-workers[115] reported in 2010 a nanoemulsion with an average particle size of 170 nm containing a PFCE core and amphiphilic Gd^{3+} chelates (Gd−DOTA−DSPE) emulsified in water using 1,2-distearoyl-*sn*-glycero-3-phosphocholine (DSPC), cholesterol, and a mixture of pegylated fluorescently tagged lipids. The additional surface functionalization of this emulsion with a cyclic RGD-peptide ligand allowed enhanced internalization by human endothelial cells, over-expressing the $\alpha_v\beta_3$-integrin receptor. In this case, PFCE relaxation times were improved by the presence of gadolinium ions, and it was also possible to follow the nanoemulsion intracellular trafficking by exploiting fluorescent labeling. A better understanding of the agent's activity was gained.

The interaction between paramagnetic metals and fluorinated MRI probes has been exploited in several works, not only focused on PFCs. An interesting example, published by Yu and co-workers,[116] presented the synthesis of a fluorinated chelator (FC; Figure 15) consisting of a small, water-soluble molecule

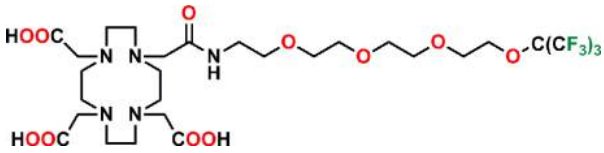

Figure 15. Chemical structure of the fluorinated chelator (FC) by Yu et al.

containing nine chemically equivalent fluorine atoms responsible for the ^{19}F signal. Yu also described the molecule chelation to several paramagnetic metal ions that modulate the ^{19}F signal and lead to a set of potential multifrequency ^{19}F imaging tracers, each giving a signal at a specific wavelength. A convenient synthesis of FC was developed, and a set of di- and trivalent metal ions chelates was easily obtained. All of them gave one single unsplit ^{19}F signal with a frequency spread of 7.89 ppm by changing the metal. Paramagnetic ions were also able to shorten ^{19}F relaxation times of the chelator, improving SNR. In this context, use of more rigid and shorter linkers between the paramagnetic center and the ^{19}F moiety could further improve the relaxation enhancement of ^{19}F by imposing a convenient separation,[23] but the need for long hydrophilic spacers is often related to solubility issues of the fluorinated probe.

An innovative approach in construction of multifunctional imaging probes exploited the unique optical properties of quantum dots (QDs), e.g., fluorescent semiconductor nanocrystals with size-dependent tunable emission in the visible and NIR regions, and high photoluminescence quantum yields.[117,118] The coupling of QDs to PFCs with different MR spectra has been reported and gave access to both multispectral MR and multicolor optical imaging modalities (Figure 16).[119] QDs with minimum spectral overlaps were incorporated into PFCs after being coated with 1*H*,1*H*,2*H*,2*H*-perfluorooctanethiol in order to increase their compatibility with fluorinated molecules. Afterward, the PFC-dispersed QDs were emulsified in water using phospholipids and emulsifying devices. The resulting nanoemulsions proved to be effective for in vivo multispectral MR and multichromic optical imaging.

The combination of gadolinium and PFCs has also been used in simultaneous acquisition of both ^{1}H and ^{19}F MR images, combining the quantitative information provided by ^{19}F and the anatomical ones coming from ^{1}H. Moreover, formulations of multimodal $^{1}H/^{19}F$ probes have been further functionalized with targeting ligands with the aim of developing quantitative assessment tools for specific pathological features.

Wickline and co-workers developed highly fluorinated nanoparticles that bind selectively to fibrin, a molecule often found in atherosclerotic plaques,[120,121] and successfully quantify it in human plasma clots and carotid samples.[122] For example, biotinylated nanoemulsions containing 20% (v/v) of fluorinated core and consisting of either PFCE or PFOB were formulated in water with lecithin, cholesterol, biotinylated dipalmitoylphosphatidylethanolamine, and a 30% mol of a lipophilic gadolinium chelate.[123] Successful binding of these particles to fibrin-containing tissues enabled both their imaging and a quantitative measurement of the agent's local concentration. The large payload characteristic of these nanodroplets (~94 200 Gd^{3+}/particle delivered to the binding sites) allowed for a very low concentration of gadolinium while providing good diagnostic contrast (Figure 17).

An even further step ahead is the fusion of diagnostic imaging and therapeutic treatment, leading to the so-called "theranostic" agents.[124] Ideally, if an agent could provide precise information about a disease by specifically targeting abnormal cells and/or tissues and, at the same time, selectively deliver the required drug(s) then the prognosis of several currently incurable diseases would be significantly improved. One of the clinical fields that can greatly benefit from this possibility is undoubtedly oncology. Anticancer drugs are usually small molecules with almost no targeting properties, thus resulting in low therapeutic efficacy and severe side effects. If these molecules could be delivered directly

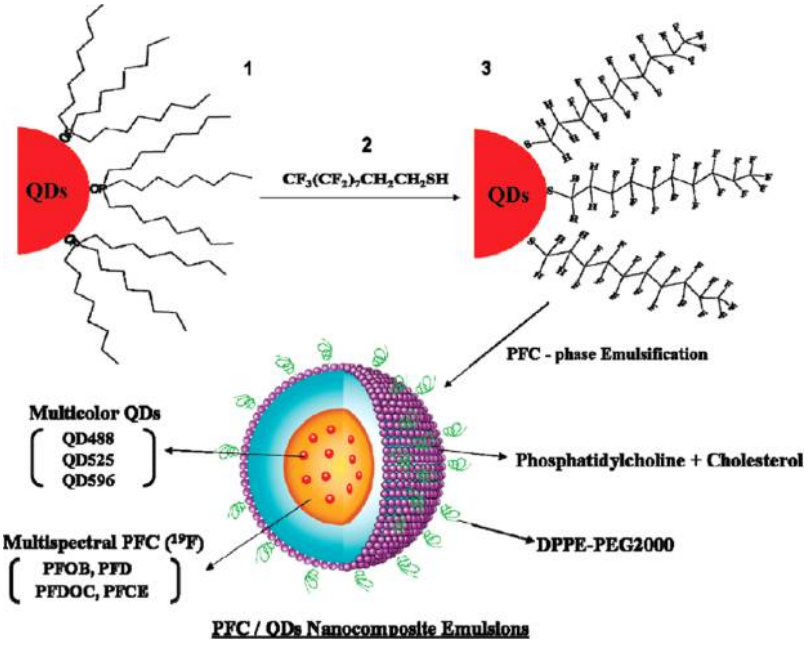

Figure 16. Representation of bimodal fluorinated nanoprobes preparation. QDs ligands (1) were exchanged with 1*H*,1*H*,2*H*,2*H*-perfluorodecanethiol (2), and the obtained QDs (3) were incorporated into PFC_S. PFC-dispersed QDs were emulsified in water, yielding nanoemulsions having both ^{19}F-based and multispectral magnetic resonance. Reprinted with permission from ref 119. Copyright 2009 American Chemical Society.

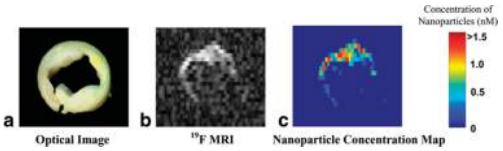

Figure 17. (a) Optical image of a cross-section of a human carotid endarterectomy sample. (b) ^{19}F projection image acquired at 4.7 T through the carotid artery. (c) Concentration map of bound nanoparticles in the carotid sample. Reprinted with permission from ref 123. Copyright 2004 John Wiley and Sons.

to cancerous cells, their efficacy would be highly amplified with a significant reduction of their side effects.[125] Furthermore, theranostics would allow cancer therapy to be tailored to individual patient's needs, as required by personalized care. Consequently, it is not surprising that recent literature shows a tremendous increase of interest in multimodal agents for cancer therapy. These agents are typically obtained by assembling one or more imaging probes, a targeting agent, and a drug.[5]

The potential of target binding of fluorinated nanoparticles has been exploited since the early stages for targeted drug delivery. For example, lipophilic antiproliferative agents with different water solubilities, such as doxorubicin (highly water soluble) or paclitaxel (poorly water soluble), were introduced in the surfactant comixture used in water nanoemulsions containing Gd−DTPA−BOA, a biotinylated phosphatidylethanolamine, and a PFOB core. A final particle size of 250 nm was obtained.[126] These particles, selectively bound to medial smooth muscle cells, were detected with both ^{19}F MRI and intravascular ultrasound imaging and, at the same time, allowed for targeted delivery of drugs directly within vascular walls.

Another interesting combination of ^{19}F MRI, paramagnetic metal ions, and the therapeutic agent consisted in the coating of magnetic and paramagnetic metallic nanoparticles with fluorinated polymers simultaneously containing 5-fluorouracil, an antiviral drug. In this study by Chu and co-workers, poly(HFMA-*g*-PEGMA), an amphiphilic fluorinated polymer, was used to coat oleic acid-stabilized magnetite NPs and disperse them in aqueous media.[127] The fluorinated segment of the polymer, which was essential to interact with hydrophobic oleic acid chains, was also effective for drug loading using 5-fluorouracil. The obtained NPs were suitable for in vivo applications.

Chemical exchange saturation transfer (CEST) is another technique that can benefit from the use of innovative theranostic agents. It is based on proton exchange processes that alter the signal of water in living tissues generating a contrast enhancement in ^{1}H MRI.[128] Classic performing agents in this method are lipid-based nanoformulations, called lipoCEST, which provide rapid exchange of magnetically labeled water molecules across the phospholipid membrane and transfer the signal saturation to the water contained in the tissues.[129]

Recently, the CEST technique has been coupled with ^{19}F MRI in several studies. In one of the first reports on this a temperature-sensitive liposomal ^{1}H CEST with ^{19}F MRI contrast agent was studied for potential targeted drug delivery applications.[130] Such liposomes contained in their water pool the chemical shift agent, thulium(III) 10-(2-hydroxypropyl)-1,4,7,10-tetraazacyclododecane-1,4,7-triacetate monohydrate [Tm(hpdo3a)(H_2O)], and in the lipid bilayer the fluorinated probe, NH_4PF_6. At the melting point of the lipid membrane, the chemical shift agent was released, thus relieving the fluorinated probe from its influence, as evidenced by the appearance of a ^{19}F signal (Figure 18).

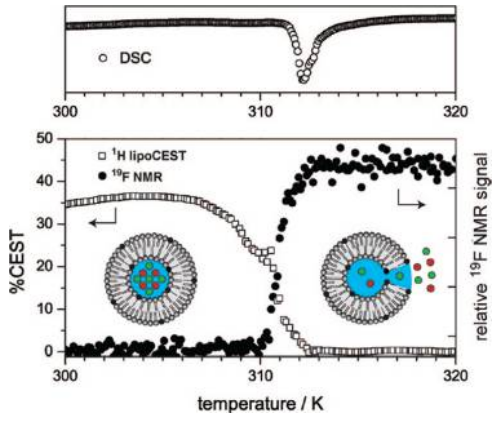

Figure 18. DSC thermogram shows the melting endothermic peak of the lipid membrane (top). The ^{1}H CEST effect and ^{19}F NMR signal intensity of the temperature-sensitive liposomal contrast agent containing [Tm(hpdo3a)(H_2O)] and NH_4PF_6 as a function of temperature (bottom). Reprinted with permission from ref 130. Copyright 2009 American Chemical Society.

More complex systems, combining several imaging techniques, have been reported as suitable for drug delivery. The first theranostic agent combining ^{19}F MRI and near-infrared fluorescence (NIRF) for simultaneous drug delivery and macrophage tracking was published in 2013 by Janjic and co-workers.[131] These o/w nanoemulsions, composed of a mixture of nonionic surfactants and PFPE as fluorinated probe, contained simultaneously CellvueH NIR815 or Burgundy as NIRF dye and Celecoxib (a nonsteroidal anti-inflammatory drug, able to inhibit cyclooxygenase-2 enzymes).[132] The final nanodroplets successfully encapsulated the drug and effectively delivered it to macrophages, inhibiting production and release of prostaglandin E_2, which is known to promote tumor growth.[133]

Targeting the activity of enzymes strongly related to certain diseases is an effective strategy to monitor the disease itself. hMAO-A (monoamine oxidase A) is an enzyme that oxidizes monoamine neurotransmitters and is thought to be related to depression (inhibitors of this enzyme are currently prescribed as antidepressants).[134−136] Interestingly, a ^{19}F MRI probe able to monitor its activity was reported in 2011. This probe contained a fluorinated hMAO-A inhibitor analog, which provided selective binding together with a source of ^{19}F NMR signal (Figure 19).[137] In the presence of hMAO-A, the amino group of this molecule was oxidized, a propanal moiety was then released, and a change in the fluorine nuclei chemical shifts was observed.

A last category of "smart" imaging tools consists of stimuli-responsive probes whose MR signal can be switched on or off by a change in pH or oxygen or metal ion concentration or by contact with a certain molecule (enzyme, marker, antibody, etc.).[138,139] Due to their specificity, these agents have a wide range of applications and are particularly useful for quantifying parameters that influence their response.[14]

Various fluorinated peptides have been reported wherein a CF_3 group is on one end and a Gd^{3+} chelate on the other end. These peptides can be engineered so that an internal bond is selectively cleaved by a specific kind of protease, and the fluorinated moiety is released. This enzymatic cleavage significantly reduces the effect of paramagnetic relaxation enhancement by gadolinium on fluorine, leading to an increase in T_2 and a clear signal enhancement.[140,141]

A peculiar approach was recently used by Sando and co-workers in the design of a novel probe for binding of endogenous

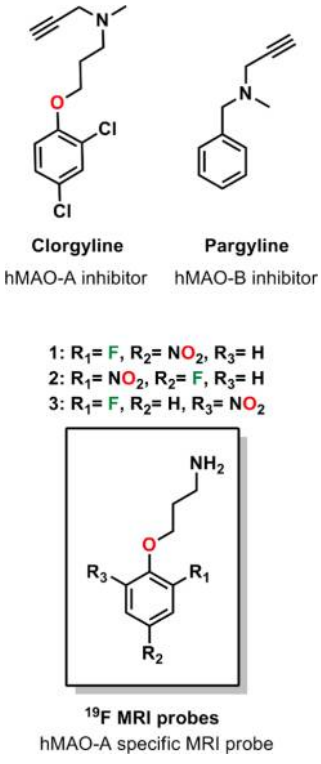

Figure 19. Structures of typical MAO inhibitors (top) and chemically related ^{19}FMRI probes.

biomaterials, such as blood.[142] Blood has a high content of serum albumin (about 50% of total proteins), which typically offers binding sites for small hydrophobic molecules. Adherence to albumin causes a shortening of the molecule T_2 due to its lowered mobility. On the basis of this concept and exploiting the hydrophobicity of fluorinated compounds, this team has designed an agent able to react with hypochlorous acid contained in human serum albumin (HSA), which is a known biomarker of inflammatory diseases (Figure 20).[143,144] The reaction product, more hydrophilic than the starting compound, shows a remarkably increased T_2 value. This novel agent was successfully applied to the detection of myeloperoxidase, an enzyme found in neutrophils and strongly linked to cardiovascular and neurodegenerative diseases.[145]

A last and very interesting example of a pH-responsive fluorinated probe has been reported by Waggoner and his group.[146] A PFPE methyl ester was covalently bound to CypHer5, a pH-sensitive cyanine derivative (Figure 21),[147,148] and then formulated in water to give a highly fluorinated nanoemulsion containing a pH-responsive fluorochrome. This newly developed agent was applied to intracellular pH measurements in living cells through simultaneous use of flow cytometry, fluorescence microscopy, and ^{19}F MRI.

Research is focusing more and more on the development of multifunctional tools to simultaneously acquire different kinds of information, improving the chances of early diagnosis of diseases and of targeted delivery of treatments specifically tailored for the patient. This is the ultimate goal of the efforts of a growing number of scientists in several different disciplines, and ultimately these are the agents that have been pushed forward from mere studies and proofs of concepts to applications in vivo and even in clinical trials. In the last section of this review we will focus on the results achieved when ^{19}F MRI has actually been applied to different kind of treatments.

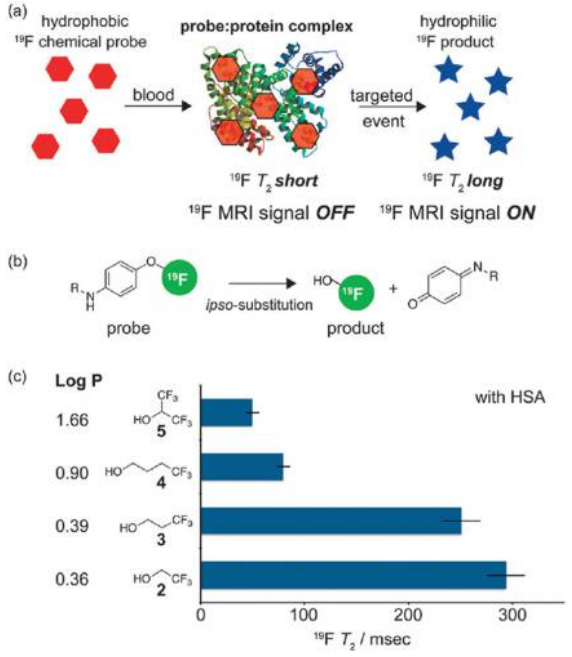

Figure 20. Schematic representation of a targeted biological event sensing through the use of a signal off-to-on-type ^{19}F MRI chemical probe (a). Chemical details on the release of the fluorinated portion from the probe (b). Log *P* values of compounds 2−5 in phosphate buffer (pH 7.4) as a function of their ^{19}F T_2 values (c). Reprinted with permission from ref 142. Copyright 2013 Royal Society of Chemistry.

5. APPLICATIONS

As extensively discussed in the previous sections, the low amount of fluorine in the human body makes ^{19}F MRI a particularly performing technique, as the resulting MR images are only due to the administered tracers. On the other hand, clinical applications of fluorinated CAs are still very limited, as the viable concentration of such tracers still results in sensitivity issues.[12,29,149] In this section, we offer a brief account of how the reviewed tracers are currently being used in preclinical and clinical studies. Biomedical applications of the most promising ^{19}F MRI probes will be grouped in three main categories according to their different clinical targets. We will initially focus on the targeted imaging of selected physiological features; then we will move to the more recent fields of cell tracking and targeted drug delivery.

5.1. Targeted Imaging of Selected Relevant Physiological Features

Selective imaging of certain tissues or organs is the most direct among all possible clinical applications of MRI. The aim here is to develop noninvasive tools for early diagnosis of diseases and medical treatment follow up.[150]

Major attention has been given to the MR imaging of angiogenesis, a critical early feature of atherosclerotic plaque development, and of the pathogenesis of aortic valve stenosis, which plays a key role also in tumor growth and therapy. Most of these MRI studies were performed using PFOB- or PFCE-based nanoemulsions containing ligands able to target integrins, biomarkers directly linked to angiogenesis, in order to selectively visualize the affected tissues.[151−153]

PFC-based CAs have been also widely used to detect inflammation, a pathological marker strictly associated with several human diseases.[154] For example, several groups

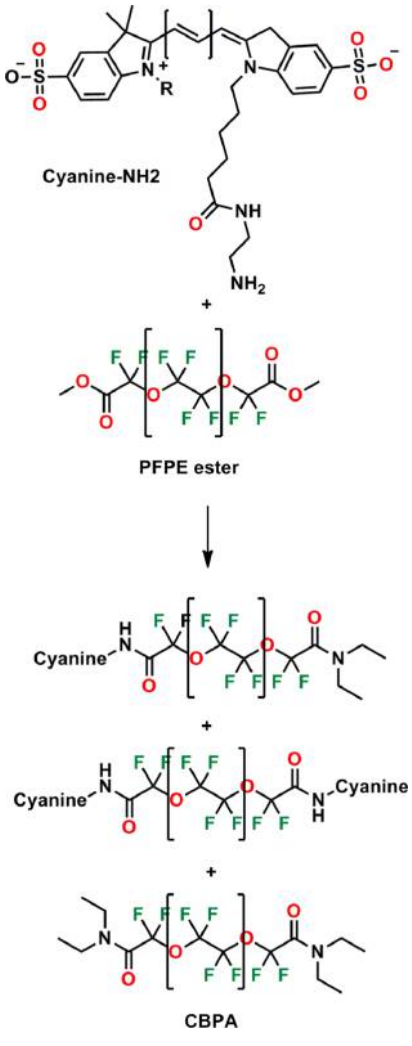

Figure 21. Synthetic scheme of pH-responsive CBPA.

succeeded in the in vivo ^{19}F MR imaging of inflammatory processes. They generally used PFCE nanoemulsions able to permanently label monocytes and macrophages, whose number is found to increase in inflamed tissues (Figure 22).[155−159]

The results obtained so far in the in vivo tumor imaging by ^{19}F MRI are very preliminary. We cite here the PFOB-containing and long-circulating PLGA−PEG nanocapsules that were successfully exploited for imaging spleen, liver, and colon carcinoma cells.[71] More recently, PEG-based fluorinated hyperbranched polymers were used for in vivo detection of B16 melanoma cells by means of $^{19}F/^{1}H$ MRI combined with fluorescence imaging.[85]

Quantitative proxy measurements are another interesting application. They are based on the correlation between the NMR response of fluorinated probes and certain physiological parameters. Quantitative ^{19}F MRI of PFCs has been extensively investigated for in vivo mapping of tissue oxygenation, since at any given temperature the partial pressure of dissolved O_2 (pO_2) in PFCs is linearly correlated with their ^{19}F longitudinal relaxivity R_1 ($1/T_1$). Several studies have been reported focusing on quantification of blood or intracellular pO_2.[44,68,160,161] Tissue oxygenation is of particular interest in oncology: due to the poorly organized vasculature and high oxygen consumption typical of cancer cells, local hypoxia is commonly associated with the presence of tumors and is also known to decrease the efficacy of radiotherapy and chemotherapy. In vivo studies of tumor oxygenation levels have been carried out since the late 1990s.[44,45,162] Recently, intracellular pO_2 of central nervous system (CNS) glioma cells was successfully measured in vivo, and it proved useful for possible monitoring of chemotherapy efficacy in CNS glioma.[163]

Several research efforts on quantitative ^{19}F MRI have focused on "stimuli-responsive" or "on−off" applications, where the NMR signal of fluorinated contrast agents can be selectively activated by an external stimulus. In this field, most studies are focused on pH-sensitive tracers, since pH is an important physiological parameter in both intracellular and extracellular milieu. These tracers generally show a strong change in their imaging performances at specific pH values, and this characteristic might be exploited for detecting local pH changes in vivo.[83,84,164] Although these results are very encouraging, no in vivo data have been reported to date. Development of enzyme-sensitive probes has been also investigated. The ^{19}F MR signal of these agents can be modulated by an enzymatic reaction, either displaying a chemical shift change or showing a signal turn on due to paramagnetic relaxation enhancement. Intracellular reductases are enzymes involved in tumor hypoxia-selective processes, and a fluorinated probe sensitive to these enzymes was, for example, developed by Nishimoto and co-workers.[165] After reacting with such enzymes, the fluorinated portion of the probe is released, thus producing a sharp ^{19}F MR signal. Also, supramolecular self-assembly of fluorinated tracers can induce changes in ^{19}F T_2. For example, the presence of a target protein has been shown to cause the disassembling of supramolecular fluorinated NPs, producing a sharp characteristic ^{19}F NMR signal.[166] In all these cases, where a "smart" on/off switch needs to be followed in vivo to track a

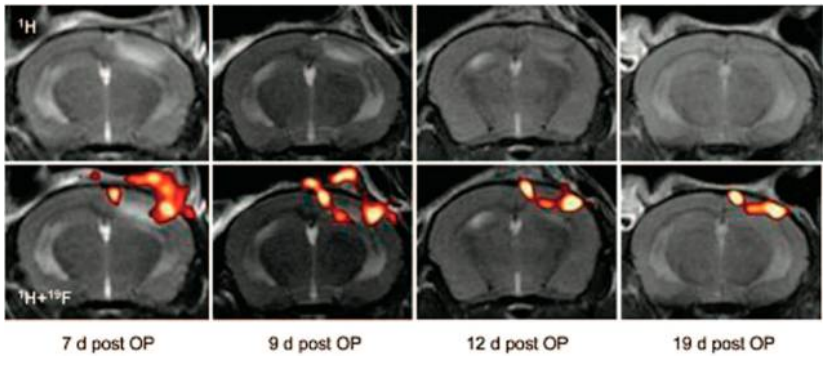

Figure 22. Infiltration of PFCs into the brain after induction of focal cerebral ischemia by photothrombosis, showing movement of the PFCs with the rim of the infarct over time. Reprinted with permission from ref 155. Copyright 2008 Wolters Kluwer Health.

biological function, it is essential that the concentration of the active molecule reaches the threshold detectable at the clinical scanning fields. For this reason, great efforts from many research groups are now devoted to optimize the chemical structure of these functional probes for increasing their water solubility and intracellular retention time.

Although several goals have been achieved, a decisive but still unreached one is the development of CAs suited for simultaneous detection and/or quantification of multiple disease biomarkers. This goal would be extremely useful for characterization of complex pathological cases.

5.2. Targeted Drug Delivery

A wide range of already approved drugs contains fluorine atoms[167] which can be directly followed via ^{19}F MRI allowing their localization and metabolism in the organism to be monitored in a quantitative way.

It is known that there is a direct link between drugs pharmacodynamics and targeting to their site of action. The possibility of measuring the effectiveness of targeting in vivo would thus provide insights on the mechanism of action of such drugs.[168] In this regard, ^{19}F MRI permits direct detection of drugs pharmacokinetics in targeted tissues and quantitative measurement of their concentration and of possible chemical modifications, which is particularly interesting for highly toxic drugs such as anticancer ones.[169]

Many in vitro studies have been recently reported on the use of ^{19}F MR for imaging of targeted drug delivery thanks to the development of novel fluorinated theranostic agents (see section 4) which contain highly fluorinated shells able to incorporate hydrophobic drugs. For example, antiproliferative agents, such as doxorubicin and paclitaxel, have been encapsulated into a PFOB nanoemulsion and delivered directly into the vascular walls. Monitoring and quantitative analysis of the delivery were successfully carried out via ^{19}F MRI.[126] In a similar way, a COX-2 inhibitor and a NIRF agent were incorporated into PFC nanoemulsions which were successfully used for drug delivery and monitoring of the macrophage interaction with tumors.[131]

Simultaneous targeted drug delivery and ^{19}F MRI monitoring is still an open and quite challenging field. Most of the reports showed only in vitro proof-of-concept investigations, and even if its feasibility has already been proved, targeted drug delivery by means of ^{19}F contrast agents is still quite far from a real applicability in humans.

5.3. Cell Tracking and Trafficking

Cell tracking and trafficking is definitely a very promising field. Cell therapy is a growing field, which promises to dramatically change in the near future the way we look at a wide range of serious illnesses and treat them, from chronic and degenerative conditions to neurological and genetic disorders.[170]

Several laboratories have been developing methodologies to apply MRI to cell imaging and tracking. Superparamagnetic iron oxide NPs and gadolinium-based contrast agents were initially used,[171,172] but more recently, the field has been flooded with studies on the use of PFCs as cell-labeling agents, particularly as ^{19}F MRI is quite suitable for quantitative measurements.[51,65]

Cell labeling can either happen in vivo, by systemically administering the agent of choice to the subject, or ex vivo, by transferring the cells to the subject after incubating them with the agent. In this latter case the incubation period is the determining step: a high cellular uptake is critical for viable images, and several factors can affect it, first of all the NP sizes. The ex vivo approach is more widely used than in situ administration because it allows a more precise and reproducible labeling and it offers, at the same time, the opportunity to select the desired cell phenotypes. A further advantage of this technique is the very low amount of needed tracer when compared with systemic administration. However, it is worth noting that it is still not possible to discern whether the signal registered is coming from the CA within an alive and a completely functional cell, or if a modification in cellular activity, or even apoptosis occurred after injection. Ex vivo studies of labeled tissues are needed to know with certainty the exact positioning of the label.[173]

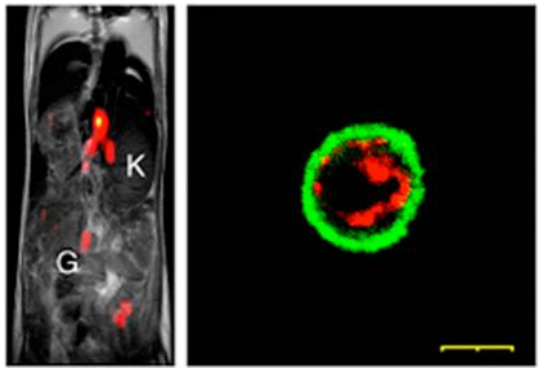

Figure 23. In vivo MR imaging of T cells labeled with a fluorescently tagged PFC nanoemulsion. Labeled cells in the lymph nodes (left); fluorescence microscopy of a single labeled cell (right). Reprinted with permission from ref 51. Copyright 2013 John Wiley and Sons.

Dendritic cells (DCs), stem cells (SCs), and T cells have undoubtedly been used widely in cell-tracking studies. DCs are of particular interest for their ability to easily internalize a wide range of agents and to initiate immune responses; SCs play a fundamental role in regenerative therapeutics; T cells are directly linked to autoimmune diseases. Their abnormal trafficking is directly linked to diseases like diabetes and lupus, and imaging of these patterns would be very beneficial for the understanding of these illnesses (Figure 23).

PFCs nanoemulsions have been the first CAs to be explored and those affording the most interesting results, with several of them being commercialized and used for preclinical and clinical studies. Studies using PFCE and Cell Sense nanoemulsions have stood up among all those reported in the last 10 years for the possible translation into human applications. One of the first reports of preclinical studies with CS-1000 showed, in fact, the labeling of human DCs, which were then successfully imaged in vivo via ^{19}F MRI.[174]

Hot-spot images of neural SCs, labeled ex vivo with differently charged PFCs nanoemulsions and transplanted in vivo, were reported (Figure 24).[175,176] Human neural SCs were effectively labeled also with CS-100 by several groups and then transplanted into mouse brains and successfully evidenced in ^{19}F MR images.[177,178]

We can thus infer that cell tracking/trafficking is the field which has afforded the most promising results among all currently reported (pre)clinical applications of ^{19}F MRI. Importantly, it is actually getting close to applications in humans as in April of 2013 the first human patient was transplanted with DCs labeled with a Cell Sense product; the Phase 1 clinical trial was cleared by the U.S. FDA.[77]

6. CONCLUSIONS

^{19}F MRI is indeed a powerful tool, and its potential has not been completely understood or exploited, yet. It can be anticipated

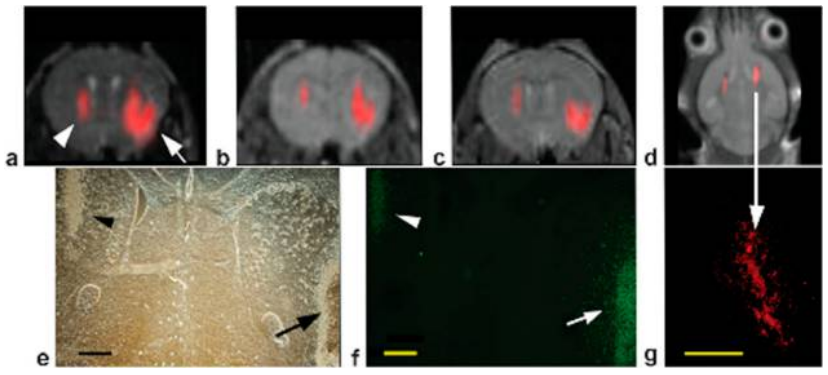

Figure 24. In vivo MR imaging of transplanted neural SCs. (a−d) In vivo images over time. (e−g) Corresponding histopathologies. Reprinted with permission from ref 176. Copyright 2008 John Wiley and Sons.

that the coming years will bring a tremendous impact of this technique on the diagnosis and treatment of human diseases. It is just as evident that ^{19}F MRI will not be able to replace the currently used imaging techniques. Its role will probably be to compensate for the shortcomings and to fill the information gaps left by other complementary diagnostic tools.

Undoubtedly, its strongest trait is the solid possibility of becoming a mean of targeted early diagnosis. The feasibility of developing accurately tailored agents able to target specific biomarkers or cells, thus reaching selected organs and/or tissues, has been extensively proved. The hot-spot kind of images provided by ^{19}F MRI can be associated with those targets and anatomically interpreted by their superimposition to images from full-body ^{1}H MRI. The value of ^{19}F MRI will tremendously increase when, and if, targeting will be effectively coupled with the ability to deliver treatment directly in the targeted sites, as a real theranostic tool will be available.

Highly fluorinated molecules have proved over the years to be highly biocompatible, with some of them being FDA approved and currently used in clinical treatments. This is a green light for the synthesis of a wide range of new fluorinated CAs. However, the chemistry of compounds containing perfluorocarbon residues frequently requires specific skills which typically come with a long experience in the field. Even then, synthesis of a truly versatile platform can be a tremendous challenge. This is probably why the number of molecules used in the hundreds of papers published in the last 20 years is quite limited. Our established experience in fluorine chemistry allowed us to design and prepare a superfluorinated contrast agent suitable for in vivo cell tracking and trafficking (Figure 1, PERFECTA). The compound possesses excellent cellular compatibility, and its spectral properties, relaxation times, and sensitivity are promising for in vivo ^{19}F MRI applications.[179]

^{19}F MRI is a relatively young technique; however, the state-of-art in the field shows a very encouraging picture, and efforts in this area may prove tremendously rewarding in the medium to long run.

AUTHOR INFORMATION

Corresponding Authors

*E-mail: francesca.baldelli@nanomedicen.eu.
*E-mail: pierangelo.metrangolo@polimi.it.
*E-mail: giuseppe.resnati@polimi.it.

Author Contributions

The manuscript was written through contributions of all authors. All authors have given approval to the final version of the manuscript.

Funding

The authors gratefully acknowledge financial support from MIUR, through the FIRB project "FLUORIMAGING" no. RBAP1183B5 and from Regione Lombardia (Fondo per lo Sviluppo e la Coesione-FAS 2007−2013).

Notes

The authors declare no competing financial interest.

ABBREVIATIONS

^{19}FIT	^{19}F imaging tracer
ATR-SCVCP	atom transfer radical self-condensing vinyl (co)-polymerization
BOA	bis-oleate
CAs	contrast agents
CCS	core cross-linked star
CEST	chemical exchange saturation transfer
CNS	central nervous system
COX	cyclooxygenase
CTA	chain transfer agent
DCs	dendritic cells
DMAEMA	2-(dimethylamino)ethyl methacrylate
DSDMA	Bis(2-methacryloyl)oxyethyl disulfide
DSPC	1,2-distearoyl-*sn*-glycero-3-phosphocholine
DTPA	diethylene-triamine-pentaacetic acid
EGDMA	ethylene glycol dimethacrilate
EYP	egg yolk phospholipids
FBPAs	fluorescent blended PFPE amides
FDA	Food and Drug Administration
HFB	hexafluorobenzene
hMAO-A	monoamine oxidase A
HSA	human serum albumin
MNP	magnetic nanoparticle
MRI	magnetic resonance imaging
MSE	multispin echo
NIR	near Infrared
NIRF	near infrared fluorescence
NMR	nuclear magnetic resonance
NPs	nanoparticles
PAMAM	poly(amidoamino)
PBS	phosphate buffer solutions
PEG	polyethylene glycole
PEI	polyethylene imine
PET	positron emission tomography
PFCE	perfluoro-15-crown-5-ether
PFCs	perfluorocarbons
PFD	perfluorodecalin
PFN	perfluorononane
PFOB	perfluorooctyl bromide
PFPEs	perfluoropolyethers
PLGA	poly(D,L-lactide-*co*-glycolide)
pO_2	pressure of dissolved O_2
PPEGMA	polyethylene glycol monomethyl ether methacrylate
QDs	quantum dots
RAFT	reversible addition−fragmentation chain transfer
RF	radiofrequency
RGD	arginylglycylaspartic acid
SCs	stem cells
SEM	scanning electron microscopy
SNR	signal to noise ratio
SPIO	superparamagnetic iron oxide
TFEMA	2,2,2-trifluoroethyl methacrylate
TFPMA	2,2,3,3-tetrafluoropropyl methacrylate

REFERENCES

(1) Lauterbur, P. C. *Nature* **1973**, *242*, 190.
(2) Debbage, P.; Jaschke, W. *Histochem. Cell. Biol.* **2008**, *130*, 845.
(3) Villaraza, A. J. L.; Bumb, A.; Brechbiel, M. W. *Chem. Rev.* **2010**, *110*, 2921.
(4) Yousaf, M. Z.; Jing, Y.; Yang-Long, H.; Song, G. *Chin. Phys. B* **2013**, *22*, 058702.
(5) Kim, J.; Piao, Y.; Hyeon, T. *Chem. Soc. Rev.* **2009**, *38*, 372.
(6) Cormode, D. P.; Jarzyna, P. A.; Mulder, W. J. M.; Fayad, Z. A. *Adv. Drug Delivery Rev.* **2010**, *62*, 329.
(7) Terreno, E.; Delli Castelli, D.; Viale, A.; Aime, S. *Chem. Rev.* **2010**, *110*, 3019.
(8) Shan, L.; Chopra, A.; Leung, K.; Eckelman, W. C.; Menkens, A. E. *J. Nanopart. Res.* **2012**, *14*, 1122.
(9) Sun, C.; Lee, J. S. H.; Zhang, M. *Adv. Drug Delivery Rev.* **2008**, *60*, 1252.
(10) Hilger, I.; Kaiser, W. A. *Nanomedicine* **2012**, *7*, 1443.
(11) Liu, G.; Gao, J.; Ai, H.; Chen, X. *Small* **2012**, *9*, 1533.
(12) Pan, D.; Lanza, G. M.; Wickline, S. A.; Caruthers, S. D. *Eur. J. Radiol.* **2009**, *70*, 274.
(13) Atanasijevic, T.; Shusteff, M.; Fam, P.; Jasanoff, A. *Proc. Natl. Acad. Sci. U.S.A.* **2006**, *103*, 14707.
(14) Knight, J. C.; Edwards, P. G.; Paisey, S. *J. RSC Adv.* **2011**, *1*, 1415.
(15) Dolbier, W. R. *Guide to fluorine NMR for organic chemists*; Wiley: Hoboken, 2009; p 4.
(16) Holland, G. N.; Bottomley, P. A.; Hinshaw, W. S. *J. Magn. Reson.* **1977**, *28*, 133.
(17) Chen, J.; Lanza, G. M.; Wickline, S. A. *WIREs Nanomed. Nanobiotechnol.* **2010**, *2*, 431.
(18) Yu, J.-X.; Hallac, R. R.; Chiguru, S.; Mason, R. P. *Prog. Nucl. Magn. Reson. Spectrosc.* **2013**, *70*, 25.
(19) Hockett, F. D.; Wallace, K. D.; Schmieder, A. H.; Caruthers, S. D.; Pham, C. T. N.; Wickline, S. A.; Lanza, G. M. *IEEE Trans. Med. Imaging* **2011**, *30*, 22.
(20) Hu, L.; Hockett, F. D.; Chen, J.; Zhang, L.; Caruthers, S. D.; Lanza, G. M.; Wickline, S. A. *J. Magn. Reson. Imaging* **2011**, *34*, 245.
(21) Keupp, J.; Rahmer, J.; Grässlin, I.; Mazurkewitz, P. C.; Schaeffter, T.; Lanza, G. M.; Wickline, S. A.; Caruthers, S. D. *Magn. Reson. Med.* **2011**, *66*, 1116.
(22) Harvey, P.; Kuprov, I.; Parker, D. *Eur. J. Inorg. Chem.* **2012**, 2015.
(23) Chalmers, K. H.; De Luca, E.; Hogg, N. H. M.; Kenwright, A. M.; Kuprov, I.; Parker, D.; Botta, M.; Wilson, J. I.; Blamire, A. M. *Chem.—Eur. J.* **2010**, *16*, 134.
(24) Chalmers, K. H.; Kenwright, A. M.; Parker, D.; Blamire, A. M. *Magn. Reson. Med.* **2011**, *66*, 931.
(25) Schmid, F.; Höltke, C.; Parker, D.; Faber, C. *Magn. Reson. Med.* **2013**, *69*, 1056.
(26) De Luca, E.; Harvey, P.; Chalmers, K. H.; Mishra, A.; Senanayake, P. K.; Wilson, P. J.; Botta, M.; Fekete, M.; Blamire, A. M.; Parker, D. *J. Biol. Inorg. Chem.* **2014**, *19*, 215.
(27) Noth, U.; Jager, L. J. E.; Lutz, J.; Haase, A. *Magn. Reson. Imaging* **1994**, *12*, 149.
(28) Zhong, J.; Mills, P. H.; Hitchens, T. K.; Ahrens, E. T. *Magn. Reson. Med.* **2013**, *69*, 1683.
(29) Ruiz-Cabello, J.; Barnett, B. P.; Bottomley, P. A.; Bulte, J. W. M. *NMR Biomed.* **2011**, *24*, 114.
(30) Díaz-López, R.; Tsapis, N.; Fattal, E. *Pharm. Res.* **2010**, *27*, 1.
(31) Berger, R.; Resnati, G.; Metrangolo, P.; Weber, E.; Hulliger, J. *Chem. Soc. Rev.* **2011**, *40*, 3496.
(32) Cametti, M.; Crousse, B.; Metrangolo, P.; Milani, R.; Resnati, G. *Chem. Soc. Rev.* **2012**, *41*, 31.
(33) Riess, J. G. *Tetrahedron* **2002**, *58*, 4113.
(34) Krafft, M. P.; Riess, J. G. *Chem. Rev.* **2009**, *109*, 1714.
(35) Riess, J. G. *Curr. Opin. Colloid Interface Sci.* **2009**, *14*, 294.
(36) Saito, N.; Liu, C.; Lodge, T. P.; Hillmyer, M. A. *Macromolecules* **2008**, *41*, 8815.
(37) Kubowicz, S.; Baussard, J.-F.; Lutz, J.-F.; Thünemann, A. F.; von Berlepsch, H.; Laschewsky, A. *Angew. Chem., Int. Ed.* **2005**, *44*, 5262.
(38) Krafft, M. P. *Acc. Chem. Res.* **2012**, *45*, 514.
(39) Li, Z.; Kesselman, E.; Talmon, Y.; Hillmyer, M. A.; Lodge, T. P. *Science* **2004**, *306*, 98.
(40) Krafft, M. P.; Riess, J. G. *J. Polym. Sci., Part A: Polym. Chem.* **2007**, *45*, 1185.
(41) Riess, J. G. *Chem. Rev.* **2001**, *101*, 2797.
(42) Joseph, P. M.; Yuasa, Y.; Kundel, H. L.; Mukherji, B.; Sloviter, H. Q. *Invest. Radiol.* **1985**, *20*, 504.
(43) Mason, R. P.; Bansal, N.; Babcock, E. E.; Nunnally, R. L.; Antich, P. P. *Magn. Reson. Imaging* **1990**, *8*, 729.
(44) Mason, R. P.; Rodbumrung, W.; Antich, P. P. *NMR Biomed.* **1996**, *9*, 125.
(45) Xia, M.; Kodibagkar, V.; Liu, H.; Mason, R. P. *Phys. Med. Biol.* **2006**, *51*, 45.
(46) Wolfson, M. R.; Shaffer, T. H. *Paediatr. Respir. Rev.* **2005**, *6*, 117.
(47) Jacoby, C.; Temme, S.; Mayenfels, F.; Benoit, N.; Krafft, M. P.; Schubert, R.; Schrader, J.; Flögel, U. *NMR Biomed.* **2014**, *27*, 261.
(48) Schwarz, R.; Schuurmans, M.; Seelig, J.; Künnecke, B. *Magn. Reson. Med.* **1999**, *41*, 80.
(49) Mattrey, R. F. *Am. J. Roentgenol.* **1989**, *152*, 247.
(50) Bisset, G. S., III; Emery, K. H.; Meza, M. P.; Rollins, N. K.; Don, S.; Shorr, J. S. *Pediatr. Radiol.* **1996**, *26*, 409.
(51) Ahrens, E. T.; Zhong, J. *NMR Biomed.* **2013**, *26*, 860.
(52) Kaneda, M. M.; Caruthers, S.; Lanza, G. M.; Wickline, S. A. *Ann. Biomed. Eng.* **2009**, *37*, 1922.
(53) Gross, G. W.; Greenspan, J. S.; Fox, W. W.; Rubenstein, S. D.; Wolfson, M. R.; Shaffer, T. H. *Radiology* **1995**, *194*, 717.
(54) Riess, J. G. *Artif. Cells, Blood Substitutes, Immobilization Biotechnol.* **2006**, *34*, 567.
(55) Ratner, A. V.; Hurd, R.; Muller, H. H.; Bradley-Simpson, B.; Pitts, W.; Shibata, J. D.; Sotak, C.; Young, S. W. *Magn. Reson. Med.* **1987**, *5*, 548.
(56) Mattrey, R. F.; Trambert, M. A.; Brown, J. J.; Young, S. W.; Bruneton, J. N.; Wesbey, G. E.; Balsara, Z. N. *Radiology* **1994**, *191*, 841.
(57) U.S. Food And Drug Administration http://www.accessdata.fda.gov/scripts/cder/drugsatfda/index.cfm?fuseaction=Search.Overview&DrugName=IMAGENT (Accessed May 6th, 2014).
(58) Shukla, H. P.; Mason, R. P.; Woessner, D. E.; Antich, P. P. *J. Magn. Reson.* **1995**, *106*, 131.
(59) Bartusik, D.; Tomanek, B. *Adv. Drug Delivery Rev.* **2013**, *65*, 1056.
(60) Giraudeau, C.; Flament, J.; Marty, B.; Boumezbeur, F.; Mériaux, S.; Robic, C.; Port, M.; Tsapis, N.; Fattal, E.; Giacomini, E.; Lethimonnier, F.; Le Bihan, D.; Valette, J. *Magn. Reson. Med.* **2010**, *63*, 1119.

(61) Ahrens, E. T.; Flores, R.; Xu, H.; Morel, P. A. *Nat. Biotechnol.* **2005**, *23*, 983.
(62) Mignion, L.; Magat, J.; Schakman, O.; Marbaix, E.; Gallez, B.; Jordan, B. F. *Magn. Reson. Med.* **2013**, *69*, 248.
(63) Kuznetsova, I. N. *Pharm. Chem. J.* **2003**, *37*, 415.
(64) Krafft, M. P.; Riess, J. G.; Weers, J. G. The Design and Engineering of Oxygen-Delivering Fluorocarbon Emulsions. In *Submicron Emulsions in Drug Targeting and Delivery*; Benita, S., Ed.; Harwood: Amsterdam, 1998; pp 235−334.
(65) Srinivas, M.; Heerschap, A.; Ahrens, E. T.; Figdor, C. G.; de Vries, I. J. M. *Trends Biotechnol.* **2010**, *28*, 363.
(66) Krylova, O. O.; Pohl, P. *Biochemistry* **2004**, *43*, 3696.
(67) Bertilla, S. M.; Thomas, J.-L.; Marie, P.; Krafft, M. P. *Langmuir* **2004**, *20*, 3920.
(68) Giraudeau, C.; Djemai, B.; Ghali, M. A.; Boumezbeur, F.; Mériaux, S.; Robert, P.; Port, M.; Robic, C.; Le Bihan, D.; Lethimonnier, F.; Valette, J. *NMR Biomed.* **2012**, *24*, 654.
(69) Neubauer, A. M.; Myerson, J.; Caruthers, S. D.; Hockett, F. D.; Winter, P. M.; Chen, J.; Gaffney, P. J.; Robertson, J. D.; Lanza, G. M.; Wickline, S. A. *Magn. Reson. Med.* **2008**, *60*, 1066.
(70) Srinivas, M.; Cruz, L. J.; Bonetto, F.; Heerschap, A.; Figdor, C. G.; de Vries, I. J. M. *Biomaterials* **2010**, *31*, 7070.
(71) Diou, O.; Tsapis, N.; Giraudeau, C.; Valette, J.; Gueutin, C.; Bourasset, F.; Zanna, S.; Vauthier, C.; Fattal, E. *Biomaterials* **2012**, *33*, 5593.
(72) Gerhardt, G. E.; Lagow, R. J. *J. Org. Chem.* **1978**, *43*, 4505.
(73) Srinivas, M.; Morel, P. A.; Ernst, L. A.; Laidlaw, D. H.; Ahrens, E. T. *Magn. Reson. Med.* **2007**, *58*, 725.
(74) Srinivas, M.; Turner, M. S.; Janjic, J. M.; Morel, P. A.; Laidlaw, D. H.; Ahrens, E. T. *Magn. Reson. Med.* **2009**, *62*, 747.
(75) Celsense. http://www.celsense.com/vsense.html (Accessed May 6th, 2014).
(76) Janjic, J. M.; Srinivas, M.; Kadayakkara, D. K. K.; Ahrens, E. T. *J. Am. Chem. Soc.* **2008**, *130*, 2832.
(77) Celsense. http://www.celsense.com/april11_first_patient.html (Accessed May 6th, 2014).
(78) Bailey, M. M.; Kline, S. R.; Anderson, M. D.; Staymates, J. L.; Berkland, C. *J. Appl. Polym. Sci.* **2012**, *126*, 1218.
(79) Nurmi, L.; Peng, H.; Seppälä, J.; Haddleton, D. M.; Blakey, I.; Whittaker, A. K. *Polym. Chem.* **2010**, *1*, 1039.
(80) Jiang, Z.-X.; Liu, X.; Jeong, E.-K.; Yu, Y. B. *Angew. Chem., Int. Ed.* **2009**, *48*, 4755.
(81) Du, W.; Nyström, A. M.; Zhang, K.; Powell, K. T.; Li, Y.; Cheng, C.; Wickline, S. A.; Wooley, K. L. *Biomacromolecules* **2008**, *9*, 2826.
(82) Thurecht, K. J.; Blakey, I.; Peng, H.; Squires, O.; Hsu, S.; Alexander, C.; Whittaker, A. K. *J. Am. Chem. Soc.* **2010**, *132*, 5336.
(83) Wang, K.; Peng, H.; Thurecht, K. J.; Puttick, S.; Whittaker, A. K. *Polym. Chem.* **2013**, *4*, 4480.
(84) Wang, K.; Peng, H.; Thurecht, K. J.; Puttick, S.; Whittaker, A. K. *Polym. Chem.* **2014**, *5*, 1760.
(85) Rolfe, B. E.; Blakey, I.; Squires, O.; Peng, H.; Boase, N. R. B.; Alexander, C.; Parsons, P. G.; Boyle, G. M.; Whittaker, A. K.; Thurecht, K. J. *J. Am. Chem. Soc.* **2014**, *136*, 2413.
(86) Tomalia, D. A.; Baker, H.; Dewald, J.; Hall, M.; Kallos, G.; Martin, S.; Roeck, J.; Ryder, J.; Smith, P. *Polym. J.* **1985**, *17*, 117.
(87) Newkome, G. R.; Yao, Z.; Baker, G. R.; Gupta, V. K. *J. Org. Chem.* **1985**, *50*, 2003.
(88) Hawker, C. J.; Fréchet, J. M. J. *J. Am. Chem. Soc.* **1990**, *112*, 7638.
(89) Kobayashi, H.; Brechbiel, M. W. *Adv. Drug Delivery Rev.* **2005**, *57*, 2271.
(90) Tomalia, D. A.; Reyna, L. A.; Svenson, S. *Biochem. Soc. Trans.* **2007**, *35*, 61.
(91) Langereis, S.; Dirksen, A.; Hackeng, T. M.; van Genderen, M. H. P.; Meijer, E. W. *New J. Chem.* **2007**, *31*, 1152.
(92) Wiener, E. C.; Brechbiel, M. W.; Brothers, H. M., II; Magin, R. L.; Gansow, O. A.; Tomalia, D. A.; Lauterbur, P. C. *Magn. Reson. Med.* **1994**, *31*, 1.
(93) Criscione, J. M.; Le, B. L.; Stern, E.; Brennan, M.; Rahner, C.; Papademetris, X.; Fahmy, T. M. *Biomaterials* **2009**, *30*, 3946.
(94) Ogawa, M.; Nitahara, S.; Aoki, H.; Ito, S.; Narazaki, M.; Matsuda, T. *Macromol. Chem. Phys.* **2010**, *211*, 1369.
(95) Ogawa, M.; Nitahara, S.; Aoki, H.; Ito, S.; Narazaki, M.; Matsuda, T. *Macromol. Chem. Phys.* **2010**, *211*, 1602.
(96) Boas, U.; Heegaard, P. M. H. *Chem. Soc. Rev.* **2004**, *33*, 43.
(97) Petros, R. A.; DeSimone, J. M. *Nat. Rev. Drug Discovery* **2010**, *9*, 615.
(98) Zhang, L.; Gu, F. X.; Chan, J. M.; Wang, A. Z.; Langer, R. S.; Farokhzad, O. C. *Clin. Pharmacol. Ther.* **2008**, *83*, 761.
(99) Lee, J. H.; Huh, Y. M.; Jun, Y.; Seo, J.; Jang, J.; Song, H. T.; Kim, S.; Cho, E. J.; Yoon, H. G.; Suh, J. S.; Cheon, J. *Nat. Med.* **2007**, *13*, 95.
(100) Na, H. B.; Song, I. C.; Hyeon, T. *Adv. Mater.* **2009**, *21*, 2133.
(101) Kooi, M. E.; Cappendijk, V. C.; Cleutjens, K.; Kessels, A. G. H.; Kitslaar, P.; Borgers, M.; Frederik, P. M.; Daemen, M.; van Engelshoven, J. M. A. *Circulation* **2003**, *107*, 2453.
(102) Lartigue, L.; Hugounenq, P.; Alloyeau, D.; Clarke, S. P.; Levy, M.; Bacri, J. C.; Bazzi, R.; Brougham, D. F.; Wilhelm, C.; Gazeau, F. *ACS Nano* **2012**, *6*, 10935.
(103) Gentilini, C.; Evangelista, F.; Rudolf, P.; Franchi, P.; Lucarini, M.; Pasquato, L. *J. Am. Chem. Soc.* **2008**, *130*, 15678.
(104) Posocco, P.; Gentilini, C.; Bidoggia, S.; Pace, A.; Franchi, P.; Lucarini, M.; Fermeglia, M.; Pricl, S.; Pasquato, L. *ACS Nano* **2012**, *6*, 7243.
(105) Daglar, B.; Aydogan, N. *Colloids Surf., A* **2013**, *419*, 257.
(106) Dass, A.; Guo, R.; Tracy, J. B.; Balasubramanian, R.; Douglas, A. D.; Murray, R. W. *Langmuir* **2008**, *24*, 310.
(107) Wilson, R. L.; Frisz, J. F.; Hanafin, W. P.; Carpenter, K. J.; Hutcheon, I. D.; Weber, P. K.; Kraft, M. L. *Bioconjugated Chem.* **2012**, *23*, 450.
(108) Brust, M.; Walker, M.; Bethell, D.; Schiffrin, D. J.; Whyman, R. *J. Chem. Soc., Chem. Commun.* **1994**, 801.
(109) Boccalon, M.; Franchi, P.; Lucarini, M.; Delgado, J. J.; Sousa, F.; Stellacci, F.; Zucca, I.; Scotti, A.; Spreafico, R.; Pengo, P.; Pasquato, L. *Chem. Commun.* **2013**, *49*, 8794.
(110) Fang, J.; Wang, H. X.; Xue, Y. H.; Wang, X. A.; Lin, T. *ACS Appl. Mater. Interfaces* **2010**, *2*, 1449.
(111) Hartmeyer, G.; Marichal, C.; Lebeau, B.; Caullet, P.; Hernandez, J. *J. Phys. Chem. C* **2007**, *111*, 6634.
(112) Matsushita, H.; Mizukami, S.; Sugihara, F.; Nakanishi, Y.; Yoshioka, Y.; Kikuchi, K. *Angew. Chem., Int. Ed.* **2014**, *53*, 1008.
(113) Louie, A. *Chem. Rev.* **2010**, *110*, 3146.
(114) Goswami, L. N.; Khan, A. A.; Jalisatgi, S. S.; Hawthorne, M. F. *Chem. Commun.* **2014**, *50*, 5793.
(115) Kok, M. B.; de Vries, A.; Abdurrachim, D.; Prompers, J. J.; Grüll, H.; Nicolay, K.; Strijkers, G. *J. Contrast Media Mol. Imaging* **2010**, *6*, 19.
(116) Jiang, Z.-X.; Feng, Y.; Yu, Y. B. *Chem. Commun.* **2011**, *47*, 7233.
(117) Michalet, X.; Pinaud, F. F.; Bentolila, L. A.; Tsay, J. M.; Doose, S.; Li, J. J.; Sundaresan, G.; Wu, A. M.; Gambhir, S. S.; Weiss, S. *Science* **2005**, *307*, 538.
(118) Biju, V.; Itoh, T.; Ishikawa, M. *Chem. Soc. Rev.* **2010**, *39*, 3031.
(119) Lim, Y. T.; Noh, Y.-W.; Cho, J.-H.; Han, J. H.; Choi, B. S.; Kwon, J.; Hong, K. S.; Gokarna, A.; Cho, Y.-H.; Chung, B. H. *J. Am. Chem. Soc.* **2009**, *131*, 17145.
(120) Constantinides, P. *J. Atheroscler. Res.* **1966**, *6*, 1.
(121) Virmani, R.; Burke, A. P.; Kolodgie, F. D.; Farb, A. *J. Interven. Cardiol.* **2003**, *16*, 267.
(122) Caruthers, S. D.; Neubauer, A. M.; Hockett, F. D.; Lamerichs, R.; Winter, P. M.; Scott, M. J.; Gaffney, P. J.; Wickline, S. A.; Lanza, G. M. *Invest. Radiol.* **2006**, *41*, 305.
(123) Morawski, A. M.; Winter, P. M.; Yu, X.; Fuhrhop, R. W.; Scott, M. J.; Hockett, F.; Robertson, J. D.; Gaffney, P. J.; Lanza, G. M.; Wickline, S. A. *Magn. Reson. Med.* **2004**, *52*, 1255.
(124) Rizzo, L. Y.; Theek, B.; Storm, G.; Kiessling, F.; Lammers, T. *Curr. Opin. Biotechnol.* **2013**, *24*, 1159.
(125) Moore, T.; Chen, H.; Morrison, R.; Wang, F.; Anker, J. N.; Alexis, F. *Mol. Pharmaceutics* **2014**, *11*, 24.
(126) Lanza, G. M.; Yu, X.; Winter, P. M.; Abendschein, D. R.; Karukstis, K. K.; Scott, M. J.; Chinen, L. K.; Fuhrhop, R. W.; Scherrer, D. E.; Wickline, S. A. *Circulation* **2002**, *106*, 2842.

(127) Li, X.; Li, H.; Liu, G.; Deng, Z.; Wu, S.; Li, P.; Xu, Z.; Xu, H.; Chu, P. K. *Biomaterials* **2012**, *33*, 3013.
(128) Zaiss, M.; Bachert, P. *Phys. Med. Biol.* **2013**, *58*, R221.
(129) Terreno, E.; Delli Castelli, D.; Aime, S. *Contrast Media Mol. Imaging* **2010**, *5*, 78.
(130) Langereis, S.; Keupp, J.; van Velthoven, J. L. J.; de Roos, I. H. C.; Burdinski, D.; Pikkemaat, J. A.; Grüll, H. *J. Am. Chem. Soc.* **2009**, *131*, 1380.
(131) Patel, S. K.; Zhang, Y.; Pollock, J. A.; Janjic, J. M. *PLoS One* **2013**, *8*, e55802.
(132) O'Hanlon, C. E.; Amede, K. G.; O'Hear, M. R.; Janjic, J. M. *J. Fluorine Chem.* **2012**, *137*, 27.
(133) Whiteside, T. L. *Cancer Immunol. Immunother.* **2014**, *63*, 67.
(134) Berry, M. D.; Juorio, A. V.; Paterson, I. A. *Prog. Neurobiol.* **1994**, *42*, 375.
(135) Youdim, M. B.; Edmondson, D.; Tipton, K. F. *Nat. Rev. Neurosci.* **2006**, *7*, 295.
(136) Edmondson, D. E.; Binda, C.; Wang, J.; Upadhyay, A. K.; Mattevi, A. *Biochemistry* **2009**, *48*, 4220.
(137) Yamaguchi, K.; Ueki, R.; Nonaka, H.; Sugihara, F.; Matsuda, T.; Sando, S. *J. Am. Chem. Soc.* **2011**, *133*, 14208.
(138) Senanayake, P. K.; Kenwright, A. M.; Parker, D.; van der Hoorn, S. K. *Chem. Commun.* **2007**, 2923.
(139) Kenwright, A. M.; Kuprov, I.; De Luca, E.; Parker, D.; Pandya, S. U.; Senanayake, P. K.; Smith, D. G. *Chem. Commun.* **2008**, 2514.
(140) Mizukami, S.; Takikawa, R.; Sugihara, F.; Hori, Y.; Tochio, H.; Wälchli, M.; Shirakawa, M.; Kikuchi, K. *J. Am. Chem. Soc.* **2008**, *130*, 794.
(141) Keliris, A.; Mamedov, I.; Hagberg, G. E.; Logothetis, N. K.; Scheffler, K.; Engelmann, J. *Contrast Media Mol. Imaging* **2012**, *7*, 478.
(142) Doura, T.; Hata, R.; Nonaka, H.; Sugihara, F.; Yoshioka, Y.; Sando, S. *Chem. Commun.* **2013**, *49*, 11421.
(143) Shepherd, S. A.; Hilderbrand, P.; Waterman, J. W.; Heinecke, R.; Weissleder; Libby, P. *Chem. Biol.* **2007**, *14*, 1221.
(144) Baldus, S.; Heeschen, C.; Meinertz, T.; Zeiher, A. M.; Eiserich, J. P.; Münzel, T.; Simoons, M. L.; Hamm, C. W. *Circulation* **2003**, *108*, 1440.
(145) Ronald, J. A. *Curr. Cardiovasc. Imaging Rep.* **2011**, *4*, 24.
(146) Patrick, M. J.; Janjic, J. M.; Teng, H.; O'Hear, M. R.; Brown, C. W.; Stokum, J. A.; Schmidt, B. F.; Ahrens, E. T.; Waggoner, A. S. *J. Am. Chem. Soc.* **2013**, *135*, 18445.
(147) Briggs, M. S.; Burns, D. D.; Cooper, M. E.; Gregory, S. J. *Chem. Commun.* **2000**, 2323.
(148) Cooper, M. E.; Gregory, S.; Adie, E.; Kalinka, S. *J. Fluoresc.* **2002**, *12*, 425.
(149) Yim, H.; Seo, S.; Na, K. *J. Nanomater.* **2011**, *2*, 1.
(150) Yu, J.; Kodibagkar, V. D.; Cui, W.; Mason, R. P. *Curr. Med. Chem.* **2005**, *12*, 819.
(151) Schmieder, A. H.; Caruthers, S. D.; Zhang, H.; Williams, T. A.; Robertson, J. D.; Wickline, S. A.; Lanza, G. M. *FASEB J.* **2008**, *22*, 4179.
(152) Waters, E. A.; Chen, J.; Allen, J. S.; Zhang, H.; Lanza, G. M.; Wickline, S. A. *J. Cardiovasc. Magn. Reson.* **2008**, *10*, 43.
(153) Giraudeau, C.; Geffroy, F.; Mériaux, S.; Boumezbeur, F.; Robert, P.; Port, M.; Robic, C.; Le Bihan, D.; Lethimonnier, F.; Valette, J. *Angiogenesis* **2013**, *16*, 171.
(154) Stoll, G.; Basse-Lüsebrink, T.; Weise, G.; Jakob, P. *WIREs Nanomed. Nanobiotechnol.* **2012**, *4*, 438.
(155) Flögel, U.; Ding, Z.; Hardung, H.; Jander, S.; Reichmann, G.; Jacoby, C.; Schubert, R.; Schrader, J. *Circulation* **2008**, *118*, 140.
(156) Ebner, B.; Behm, P.; Jacoby, C.; Burghoff, S.; French, B. A.; Schrader, J.; Flögel, U. *Circ. Cardiovasc. Imaging* **2010**, *3*, 202.
(157) Cyrus, T.; Abendschein, D. R.; Caruthers, S. D.; Harris, T. D.; Glattauer, V.; Werkmeister, J. A.; Ramshaw, J. A. M.; Wickline, S. A.; Lanza, G. M. *J. Cardiovasc. Magn. Reson.* **2006**, *8*, 535.
(158) Schmieder, A. H.; Wang, K.; Zhang, H.; Senpan, A.; Pan, D.; Keupp, J.; Caruthers, S. D.; Wickline, S. A.; Shen, B.; Wagner, E. M.; Lanza, G. M. *Angiogenesis* **2014**, *17*, 51.
(159) Winter, P. M.; Caruthers, S. D.; Kassner, A.; Harris, T. D.; Chinen, L. K.; Allen, J. S.; Lacy, E. K.; Zhang, H.; Robertson, D.; Wickline, S. A.; Lanza, G. M. *Cancer Res.* **2003**, *63*, 5838.
(160) Eidelberg, D.; Johnson, G.; Tofts, P. S.; Dobbin, J.; Crockard, H. A.; Plummer, D. *J. Cereb. Blood Flow Metab.* **1988**, *8*, 276.
(161) Nöth, U.; Morrissey, S. P.; Deichmann, R.; Adolf, H.; Schwarzbauer, C.; Lutz, J.; Haase, A. *Magn. Reson. Med.* **1995**, *34*, 738.
(162) McNab, J. A.; Yung, A. C.; Kozlowski, P. *MAGMA* **2004**, *17*, 288.
(163) Kadayakkara, D. K. K.; Janjic, J. M.; Pusateri, L. K.; Young, W.-B.; Ahrens, E. T. *Magn. Reson. Med.* **2010**, *64*, 1252.
(164) Huang, X.; Huang, G.; Zhang, S.; Sagiyama, K.; Togao, O.; Ma, X.; Wang, Y.; Li, Y.; Soesbe, T. C.; Sumer, B. D.; Takahashi, M.; Sherry, A. D.; Gao, J. *Angew. Chem., Int. Ed.* **2013**, *52*, 8074.
(165) Tanabe, K.; Harada, H.; Narazaki, M.; Tanaka, K.; Inafuku, K.; Komatsu, H.; Ito, T.; Yamada, H.; Chujo, Y.; Matsuda, T.; Hiraoka, M.; Nishimoto, S. *J. Am. Chem. Soc.* **2009**, *131*, 15982.
(166) Takaoka, Y.; Sakamoto, T.; Tsukiji, S.; Narazaki, M.; Matsuda, T.; Tochio, H.; Shirakawa, M.; Hamachi, I. *Nat. Chem.* **2009**, *1*, 557.
(167) Wang, J.; Sánchez-Roselló, M.; Aceña, J. L.; del Pozo, C.; Sorochinsky, A. E.; Fustero, S.; Soloshonok, V. A.; Liu, H. *Chem. Rev.* **2014**, *114*, 2432.
(168) Wolf, W. W.; Presant, C. A. C.; Waluch, V. V. *Adv. Drug Delivery Rev.* **2000**, *41*, 55.
(169) Griffiths, J. R.; Glickson, J. D. *Adv. Drug Delivery Rev.* **2000**, *41*, 75.
(170) Trounson, A.; Thakar, R. G.; Lomax, G.; Gibbons, D. *BMC Med.* **2011**, *9*, 52.
(171) Yeh, T. C.; Zhang, W.; Ildstad, S. T.; Ho, C. *Magn. Reson. Med.* **1993**, *30*, 617.
(172) Bulte, J. W. M.; Arbab, A. S.; Douglas, T.; Frank, J. A. *Methods Enzymol.* **2004**, *386*, 275.
(173) Janjic, J. M.; Ahrens, E. T. *WIREs Nanomed. Nanobiotechnol.* **2009**, *1*, 492.
(174) Bonetto, F.; Srinivas, M.; Heerschap, A.; Mailliard, R.; Ahrens, E. T.; Figdor, C. G.; de Vries, I. J. M. *Int. J. Cancer* **2010**, *129*, 365.
(175) Partlow, K. C.; Chen, J.; Brant, J. A.; Neubauer, A. M.; Meyerrose, T. E.; Creer, M. H.; Nolta, J. A.; Caruthers, S. D.; Lanza, G. M.; Wickline, S. A. *FASEB J.* **2007**, *21*, 1647.
(176) Ruiz-Cabello, J.; Walczak, P.; Kedziorek, D. A.; Chacko, V. P.; Schmieder, A. H.; Wickline, S. A.; Lanza, G. M.; Bulte, J. W. M. *Magn. Reson. Med.* **2008**, *60*, 1506.
(177) Boehm-Sturm, P.; Mengler, L.; Wecker, S.; Hoehn, M.; Kallur, T. *PLoS One* **2011**, *6*, e29040.
(178) Bible, E.; Dell'Acqua, F.; Solanky, B.; Balducci, A.; Crapo, P. M.; Badylak, S. F.; Ahrens, E. T.; Modo, M. *Biomaterials* **2012**, *33*, 2858.
(179) Tirotta, I.; Mastropietro, A.; Cordiglieri, C.; Gazzera, L.; Baggi, F.; Baselli, G.; Bruzzone, M. G.; Zucca, I.; Cavallo, G.; Terraneo, G.; Baldelli Bombelli, F.; Metrangolo, P.; Resnati, G. *J. Am. Chem. Soc.* **2014**, *136*, 8524.